Department of AERONAUTICS and ASTRONAUTICS
STANFORD UNIVERSITY

S. C. McIntosh, Jr.

Theoretical Considerations of Some Nonlinear Aspects of Hypersonic Panel Flutter

Nov
1974

Final Report
NASA Grant NGR 05-020-102
(1 September 1965 to 31 August 1970)

SUDAAR
No. 491

TABLE OF CONTENTS

LIST OF ILLUSTRATIONS

NOMENCLATURE

a	Panel chord
$\bar{a}_k$	Modal amplitude for panel transverse displacement $$\bar{w}(x,t) = \sum_{k=1}^{N} \bar{a}_k(t) \sin \frac{k\pi x}{a}$$
a_k	Dimensionless modal amplitude, $\bar{a}_k/h$
$\tilde{a}_k$	Scaled modal amplitude, $(\alpha)^{\frac{1}{2}} a_k$
$\vec{A}_0$	Vector of initial modal amplitudes and velocities, $[a_1(0), \ldots, a_N(0), \dot{a}_1(0), \ldots, \dot{a}_N(0)]$
$\vec{b}_R$, $\vec{b}_0$, $\vec{b}_k$	Modal amplitudes for in-plane displacement
c_k	Dependent variable obtained by applying variation of parameters to governing panel equations
$\bar{c}_k$	Variable c_k, transformed according to Kamel's perturbation method
$\bar{c}_{1,0}$	Initial magnitude of $\bar{c}_k$
C_k^{ℓ}	Combinatorial coefficient, $\frac{\ell!}{k!(\ell-k)!}$
C_1, C_2	Cubic terms in panel governing equations
D	Plate modulus, $Eh^3/12(1-\nu^2)$
D_1	Complex constant defined in Eq. (6.27), $D_{1R} + iD_{1I}$
D_2	Complex constant defined in Eq. (6.26), $D_{2R} + iD_{2I}$
D_R	Real constant, D_{1R}/D_{2R}

E	Modulus of elasticity
$\bar{E}$	Panel total energy
E'	Dimensionless panel energy, $\bar{E}a^3/Dh^2$
$\vec{f}_k$	Perturbation coefficient vectors – see Eqs. (6.5)
$f_{k,\ell}$	ℓth component of $\vec{f}_k$
F_x	In-plane generalized force
F_z	Transverse generalized force
$\vec{g}^{(k)}$	Perturbation coefficient vectors – see Eqs. (6.1)
$g_\ell^{(k)}$	ℓth component of $\vec{g}^{(k)}$
h	Panel thickness
i	$(-1)^{\frac{1}{2}}$
K	Running spring constant, panel in-plane restraint spring
M	Free-stream Mach number
N	Number of modes used to approximate panel transverse deflection
p	Pressure
p_∞	Free-stream pressure
$\overline{\Delta p}$	Static pressure difference across panel; positive if cavity pressure exceeds free-stream pressure
Δp	Dimensionless static pressure difference, $\overline{\Delta p}a^4/Dh$
$\tilde{\Delta} p$	Scaled static pressure difference, $(\alpha)^{\frac{1}{2}}\ \Delta p$

q	Free-stream dynamic pressure, $\rho U^2/2$
Q_1 , Q_2	Quadratic terms in panel governing equations
$\bar{R}_x$	Applied in-plane load
R_x	Dimensionless in-plane load, $\bar{R}_x a^2/D$
$\bar{R}_0$	Time-varying applied in-plane load
R_0	Dimensionless in-plane load, $\bar{R}_0 a^2/D$
$\tilde{R}_0$	Scaled in-plane load, $(1 - \alpha) R_0$
t	Time
$\bar{u}$	Panel in-plane displacement
U	Free-stream speed
$\vec{U}_k$	Linear-system eigenvector at $\lambda = \lambda_c$
$U_{k,\ell}$	ℓth component of $\vec{U}_k$
$\bar{w}$	Panel transverse displacement
w	Dimensionless displacement, $\bar{w}/h$
$\vec{W}_k$	Transformation vectors defined in Eqs. (6.3)
$W_{k,\ell}$	ℓth component of $\vec{W}_k$
x	Panel in-plane coordinate
z	Panel transverse coordinate
α	In-plane restraint parameter, $K[K + Eh/a(1 - \nu^2)]^{-1}$
γ	Ratio of specific heats, $\gamma = 1.4$

ϵ	Small parameter
ϵ_1	Perturbation parameter, $(\lambda - \lambda_c)/\lambda$
ϵ_2	Perturbation parameter, $R_x/\pi^2 - \epsilon_1(1 + R_x/\pi^2)$
θ_1	Phase angle
$\theta_{1,0}$	Initial phase angle, $\theta_1(0)$
λ	Dynamic-pressure parameter, $2qa^3/MD$
λ_c	Critical value of λ determined from linear theory
μ	Mass ratio, $\rho a/\rho_m h$
ν	Poisson's ratio
ρ	Free-stream mass density
ρ_m	Panel mass density
σ_k	Eigenvalues of linear system at $\lambda = \lambda_c$
τ	Dimensionless time, $t(D/\rho h a^4)^{\frac{1}{2}}$
$\tilde{\tau}$	Scaled time, $(\lambda)^{\frac{1}{2}}\tau$
$(\dot{\ })$	Derivative of dimensional quantity with respect to t ; derivative of dimensionless quantity with respect to τ ; derivative with respect to $\tilde{\tau}$ in Section VI
$(\vec{\ })$	Vector

I. INTRODUCTION

This report constitutes a final report on research into the effects of hypersonic nonlinear aerodynamic loading on panel flutter, supported by the National Aeronautics and Space Administration under Grant NGR 05-020-102, from September 1, 1965 to August 31, 1970. The technical monitor of this grant was Mr. Peter A. Gaspers, of the Nonsteady Phenomena Branch at Ames Research Center, whose support and counsel are gratefully acknowledged.

The initial motivation for this investigation was provided by the results of some high-Mach-number panel-flutter experiments described in Ref. 1. In these experiments, in-plane tension was used to stabilize a panel until steady-state tunnel conditions were reached. The tension was reduced until flutter occurred and then increased until flutter ceased. It was noticed that the tension at which flutter ceased was in many cases consistently higher than that for which flutter occurred initially, so that there was an effect analogous to hysteresis evident in the relationship between flutter speed and in-plane tension. Such an effect is consistent with the effects of nonlinear aerodynamic loading at hypersonic speeds, which are easily and accurately represented for panels by nonlinear piston-theory aerodynamics. In general, these nonlinear aerodynamic loads are of the "soft" type, in that they produce forces augmenting any transverse panel motion. On the other hand, the more familiar geometric panel nonlinear effects are of the "hard" type, in that they produce in-plane panel loads that resist transverse displacement. It thus seemed conceivable that there would be circumstances, perhaps exemplified by the experiments in Ref. 1, where the aerodynamic nonlinear effects would in part be dominant and lead to the hysteresis effect observed. There is also the broader question of stability to large disturbances: Refs. 2 and 3 deal with this in different ways. In Ref. 2, Bolotin and co-authors showed that nonlinear hypersonic aerodynamic loads can produce situations where a panel is unstable in a parameter region where stability would be predicted with linear aerodynamic loading, provided the initial disturbance is of sufficient

magnitude. In Ref. 3, Librescu was able to demonstrate a similar effect, albeit not so precisely, with an analysis based on Lyapunov stability theory. This question was pursued further, with more realistic panel parameters, as part of the study described in this report. The effects of nonlinear aerodynamic loads on panel postcritical response were also surveyed, and results have been published in Ref. 4. The effects of aerodynamic nonlinearities on stability were evaluated by determining constant-initial-energy amplitude-sensitive stability boundaries and comparing them with the corresponding linear stability boundaries. Preliminary results were presented in Ref. 4, and a parametric survey was presented in Ref. 5. A final section treats an attempt to develop an alternative method of analysis for systems where amplitude-sensitive instability is possible; much of this section is the work of Dr. Sayed D. Hassan. More detailed summaries of work performed during the first four years of the grant period will be found in Refs. 7-10.

Another important effort supported by the grant concerned the effects of a viscous boundary layer on unsteady panel aerodynamic loading. This work is described in detail in the Ph.D. dissertation of Dr. J. I. Lerner, and is incorporated into this report by reference (Ref. 6).

The author is greatly indebted to Professors Holt Ashley, Jean Mayers, and Krishnamurty Karamcheti for many helpful discussions, to Mr. James Stein for valuable computer-programming assistance, and to Dr. Ahmed A. Kamel for consultations concerning his perturbation method.

II. EQUATIONS OF MOTION

Consider the two-dimensional panel, or plate-column, illustrated in Fig. 1. The supports are hinged, and the in-plane motion at one end is resisted by a distributed spring of constant K.* The panel is loaded by a static pressure difference $\overline{\Delta p}$, an unsteady pressure difference $p(x,t) - p_\infty$, an initial static in-plane applied load $\overline{R}_x$, and a subsequent time-varying in-plane applied load $\overline{R}_0(t)$. The unsteady pressure is approximated in hypersonic flow by a third-order piston-theory expression

$$p - p_\infty = \frac{2q}{M}\left[\frac{1}{U}\frac{\partial \overline{w}}{\partial t} + \frac{\partial \overline{w}}{\partial x} + \frac{(\gamma+1)M}{4}\left(\frac{1}{U}\frac{\partial \overline{w}}{\partial t} + \frac{\partial \overline{w}}{\partial x}\right)^2 + \frac{(\gamma+1)M^2}{12}\left(\frac{\partial \overline{w}}{\partial x}\right)^3\right] \tag{2.1}$$

A third-order term is included, because such a term will result in work done through a simple-harmonic cycle of panel motion, whereas the second-order terms will not. The pressure is assumed to act normal to the instantaneous panel surface. Since the structural representation of the panel allows for significant rotation of panel elements about a spanwise axis, order-of-magnitude consistency then dictates including as well as transverse aerodynamic loading an in-plane aerodynamic load $[(p - p_\infty)_L - \overline{\Delta p}](\partial \overline{w}/\partial x)$, where the subscript L denotes the linear portion in Eq. (2.1).

The panel transverse displacement is represented as a series of assumed modes satisfying the geometric boundary conditions of zero

*See the Nomenclature for definitions of symbols.

displacement and curvature at each end:

$$\bar{w}(x,t) = \sum_{k=1}^{N} \bar{a}_k(t) \sin \frac{k\pi x}{a} \tag{2.2}$$

A consistent assumed-mode expression for the in-plane displacement is given by

$$\bar{u}(x,t) = [\bar{b}_R + \bar{b}_0(t)] \frac{x}{a} + \sum_{k=1}^{2N} \bar{b}_k(t) \sin \frac{k\pi x}{a} \tag{2.3}$$

Here $\bar{b}_R$ is the initial panel in-plane displacement at $x = a$ due to the application of the in-plane load $\bar{R}_x$, and $\bar{b}_0(t)$ is the in-plane displacement at $x = a$ resulting from the subsequent unsteady panel motion. The reasons for this division will be discussed below.

Hamilton's principle is now used to derive the Euler-Lagrange equations of motion, as outlined in Ref. 7. The potential energy of the system is given by

$$W = \frac{1}{2} \int_0^a \left\{ \frac{Eh}{1 - \nu^2} \left[\frac{\partial \bar{u}}{\partial x} + \frac{1}{2} \left(\frac{\partial \bar{w}}{\partial x} \right)^2 \right] + D \left(\frac{\partial^2 \bar{w}}{\partial x^2} \right)^2 \right\} dx$$

$$- \left[\bar{R}_x \bar{b}_R + (\bar{R}_x + \bar{R}_0) \bar{b}_0 - \frac{1}{2} K \bar{b}_0^2 \right] \tag{2.4}$$

This expression represents the strain energy of the panel diminished by the potential of any conservative external loads. The structural representation of the panel is consistent with the assumptions of small strain, a linear stress-strain law, and element rotations whose squares are small relative to unity (see Ref. 4), and it leads to the familiar von Kármán structural operator. In the potential, it has been assumed that the restraint spring is not attached until after the load $\bar{R}_x$ is applied; this is an artifice for ensuring that in-plane tension is in the panel even

when $K = \infty$. The unknown $\bar{b}_R$ is needed simply to account for the corresponding panel displacement. This formulation also implies that the panel is initially restrained from buckling, should supercritical compressive in-plane loading be applied.

The kinetic energy is given simply by

$$T = \frac{1}{2} \rho_m h \int_0^a \left(\frac{\partial \bar{w}}{\partial t} \right)^2 dx \tag{2.5}$$

The kinetic energy associated with both in-plane motion and rotary inertia has been neglected. In-plane inertia would have to be included if parametric stability of the panel, under the load $\bar{R}_0(t)$, were to be studied. Here $\bar{R}_0$ is included only to model the varying tension used in the experiments of Ref. 1, where in-plane inertia clearly was not a factor. Rotary-inertia effects are important only if the wavelength of the panel flexural mode is comparable in magnitude to the panel thickness; such small wavelengths are not expected for panel flutter.

The transverse generalized forces are

$$(F_z)_k = \int_0^a \left[- (p - p_\infty) + \overline{\Delta p} \right] \sin \frac{k\pi x}{a} \, dx \quad , \quad k = 1,2,\ldots,N \tag{2.6}$$

Note that unsteady cavity effects, which in some cases are quite significant, are not taken into account here. The in-plane generalized forces are

$$\begin{aligned} (F_x)_0 &= \int_0^a \left[(p - p_\infty)_L - \overline{\Delta p} \right] \frac{\partial \bar{w}}{\partial x} \frac{x}{a} \, dx \\ (F_x)_k &= \int_0^a \left[(p - p_\infty)_L - \overline{\Delta p} \right] \frac{\partial \bar{w}}{\partial x} \sin \frac{k\pi x}{a} \, dx \quad , \quad k = 1,2,\ldots,2N \end{aligned} \tag{2.7}$$

The assumed-mode series for $\bar{u}$ and $\bar{w}$ are inserted in the expressions for potential energy, kinetic energy, and generalized forces. The Euler-Lagrange differential equations then become, after considerable manipulation,

$$-\frac{\partial W}{\partial \bar{b}_R} = 0 = \bar{R}_x - \frac{Eh}{a(1-\nu^2)}\bar{b}_R$$

$$-\frac{\partial W}{\partial \bar{b}_0} + (F_x)_0 = 0 = \bar{R}_x + \bar{R}_0 - K\bar{b}_0 - \frac{Eh(\bar{b}_R + \bar{b}_0)}{a(1-\nu^2)} \tag{2.8}$$

(continued)

$$- \frac{\pi^2 E_h}{4a^2(1-\nu^2)} \sum_{n=1}^{N} n^2 \bar{a}_n^2 + \frac{2q}{MU} \sum_{m,n=1}^{N} \frac{mn(-1)^{m+n}}{m^2-n^2} \bar{a}_m \dot{\bar{a}}_n - \frac{q}{2MU} \sum_{m=1}^{N} \bar{a}_m \dot{\bar{a}}_m + \frac{2q}{Ma} \sum_{m,n=1}^{N} \frac{mn(m^2+n^2)[(-1)^{m+n}-1]}{(m^2-n^2)^2} \bar{a}_m \bar{a}_n$$

$$+ \frac{\pi^2 q}{2Ma} \sum_{m=1}^{N} m^2 \bar{a}_m^2 + \frac{\overline{\Delta p}}{\pi} \sum_{n=1}^{N} \frac{1-(-1)^n}{n} \bar{a}_n \qquad (2.9)$$

$$- \frac{\partial W}{\partial \bar{b}_k} + (F_x)_k = 0 = - \frac{Eh}{1-\nu^2} \left[\frac{\pi^2 k^2}{2a} \bar{b}_k + \frac{k\pi^3}{8a^2} \left(\sum_{\substack{m,n=1 \\ m+n=k}}^{N} mn \bar{a}_m \bar{a}_n + 2 \sum_{\substack{m,n=1 \\ m-n=k}}^{N} mn \bar{a}_m \bar{a}_n \right) \right]$$

$$+ \frac{2q}{M} \left[\frac{\pi}{4U} \left(\sum_{\substack{m,n=1 \\ m+n=k}}^{N} m \bar{a}_m \dot{\bar{a}}_n - \sum_{\substack{m,n=1 \\ m-n=k}}^{N} m \bar{a}_m \dot{\bar{a}}_n + \sum_{\substack{m,n=1 \\ n-m=k}}^{N} m \bar{a}_m \dot{\bar{a}}_n \right) + \frac{k\pi}{a} \sum_{m,n=1}^{N} \frac{mn(k^2-m^2-n^2)[1-(-1)^{k+m+n}]}{[k^2-(m-n)^2][k^2-(m+n)^2]} \bar{a}_m \bar{a}_n \right]$$

$$- \overline{\Delta p} \sum_{n=1}^{N} \frac{kn[1-(-1)^{k+n}]}{k^2-n^2} \bar{a}_n \quad , \qquad k = 1,2,\ldots,2N \qquad (2.10)$$

$$- \frac{d}{dt} \left(\frac{\partial T}{\partial \dot{\bar{a}}_k} \right) - \frac{\partial W}{\partial \bar{a}_k} + (F_z)_k = 0 = - \frac{1}{2} \rho_m h a \ddot{\bar{a}}_k - \frac{Eh}{1-\nu^2} \left\{ \frac{\pi^2 k^2}{2a^2} (\bar{b}_R + \bar{b}_0) \bar{a}_k \right. \qquad \text{(continued)}$$

$$+\frac{\pi^3 k}{4a^2}\left(\sum_{\substack{m=1\\ m+n=k}}^{N}\sum_{n=1}^{2N} mn\bar{a}_m\bar{b}_n+\sum_{\substack{m=1\\ |m-n|=k}}^{N}\sum_{n=1}^{2N} mn\bar{a}_m\bar{b}_n\right)+\frac{\pi^4}{32a^3}\left[4k^2\bar{a}_k\sum_{n=1}^{N} n^2\bar{a}_n^2+4k\sum_{\substack{\ell,m,n=1\\ \ell+m-n=k,\ m\neq n}}^{N} \ell mn\bar{a}_\ell\bar{a}_m\bar{a}_n\right.$$

$$\left.\left.+2k\left(\sum_{\substack{\ell,m,n=1\\ \ell+m+n=k}}^{N} \ell mn\bar{a}_\ell\bar{a}_m\bar{a}_n+3\sum_{\substack{\ell,m,n=1\\ \ell-m-n=k}}^{N} \ell mn\bar{a}_\ell\bar{a}_m\bar{a}_n+\sum_{\substack{\ell,m,n=1\\ m+n-\ell=k}}^{N} \ell mn\bar{a}_\ell\bar{a}_m\bar{a}_n\right)\right]\right\}$$

$$-\frac{D\pi^4 k^4}{2a^3}\bar{a}_k-\frac{2q}{M}\sum_{n=1}^{N}\frac{kn[1-(-1)^{k+n}]}{k^2-n^2}\bar{a}_n-\frac{qa}{MU}\dot{\bar{a}}_k+\frac{a[1-(-1)^k]}{k\pi}\overline{\Delta p}$$

$$-\frac{(\gamma+1)q}{2}\left[\frac{k\pi}{a}\sum_{m,n=1}^{N}\frac{mn(k^2-m^2-n^2)[1-(-1)^{k+m+n}]}{[k^2-(m-n)^2][k^2-(m+n)^2]}\bar{a}_m\bar{a}_n+\frac{\pi}{2U}\left(\sum_{\substack{m,n=1\\ m+n=k}}^{N} m\bar{a}_m\dot{\bar{a}}_n\right.\right.$$

$$\left.\left.-\sum_{\substack{m,n=1\\ m-n=k}}^{N} m\bar{a}_m\dot{\bar{a}}_n+\sum_{\substack{m,n=1\\ n-m=k}}^{N} m\bar{a}_m\dot{\bar{a}}_n\right)-\frac{2ka}{\pi U^2}\sum_{m,n=1}^{N}\frac{mn[1-(-1)^{k+m+n}]}{[k^2-(m-n)^2][k^2-(m+n)^2]}\dot{\bar{a}}_m\dot{\bar{a}}_n\right]$$

(continued)

$$- \frac{(\gamma+1)qM\pi^2 k}{24a^2} \sum_{\ell,m,n=1}^{N} [1 - (-1)^{k+\ell+m+n}]$$

$$\times \left\{ [k^2 - (\ell - m - n)^2]^{-1} + 2[k^2 - (\ell - m + n)^2]^{-1} + [k^2 - (\ell + m + n)^2]^{-1} \right\} \bar{a}_\ell \bar{a}_m \bar{a}_n \quad , \quad k = 1,2,\ldots,N \qquad (2.11)$$

Multiple summations in these equations are indicated by multiple indices on a single summation sign, and the terms are arranged so that any combination of indices giving a zero denominator is to be excluded from the summation. (This convention will be observed throughout this report.) Equations (2.8) and (2.9) are used to eliminate $\bar{b}_0$, $\bar{b}_R$, and the $\bar{b}_k$ in Eqs. (2.11), and this produces a set of second-order, quasilinear ordinary differential equations governing the $\bar{a}_k$. After nondimensionalization and copious manipulation, this set becomes:

$$\frac{1}{2}\ddot{a}_k + \frac{1}{2}\left(\lambda\frac{\mu}{M}\right)^{\frac{1}{2}}\dot{a}_k + \frac{\pi^2k^2}{2}\left[R_x + (1-\alpha)R_0 + \pi^2k^2\right]a_k + \frac{3}{2}\pi^4k^2\alpha a_k\sum_{\ell=1}^{N}\ell^2a_\ell^2 + \lambda\sum_{\ell=1}^{N}\frac{k\ell[1-(-1)^{k+\ell}]}{k^2-\ell^2}a_\ell$$

$$-\frac{[1-(-1)^k]}{k\pi}\Delta p + \frac{(\gamma+1)\pi k}{4}\left(\lambda M\frac{h}{a}\right)\sum_{\ell,m=1}^{N}\frac{\ell m(k^2-\ell^2-m^2)[1-(-1)^{k+\ell+m}]}{[k^2-(\ell-m)^2][k^2-(\ell+m)^2]}a_\ell a_m$$

$$+\frac{\pi(\gamma+1)}{8}\left(M\frac{h}{a}\right)\left(\lambda\frac{\mu}{M}\right)^{\frac{1}{2}}\left[\sum_{\substack{\ell,m=1\\ \ell+m=k}}^{N}\ell\dot{a}_\ell\dot{a}_m + \sum_{\substack{\ell,m=1\\ \ell-m=k}}^{N}(m\dot{a}_m\dot{a}_\ell - \ell\dot{a}_\ell\dot{a}_m)\right]$$

$$-\frac{k(\gamma+1)}{2\pi}\left(\mu\frac{h}{a}\right)\sum_{\ell,m=1}^{N}\frac{\ell m[1-(-1)^{k+\ell+m}]}{[k^2-(\ell-m)^2][k^2-(\ell+m)^2]}\ddot{a}_\ell a_m$$

$$+\frac{\pi^2k}{2}\left(\lambda\frac{h^2}{a^2}\right)\left\{\sum_{\ell,m,n=1}^{N}\frac{\ell mn[(k-\ell)^2-m^2-n^2][1-(-1)^{k+\ell+m+n}]}{[(k-\ell)^2-(m-n)^2][(k-\ell)^2-(m+n)^2]}a_\ell a_m a_n\right.$$

$$\left.+\sum_{\ell,m,n=1}^{N}\frac{\ell mn[(k+\ell)^2-m^2-n^2][1-(-1)^{k+\ell+m+n}]}{[(k+\ell)^2-(m-n)^2][(k+\ell)^2-(m+n)^2]}a_\ell a_m a_n\right\}$$

(continued)

$$+ k^2 a_k \frac{\pi^2}{2}\left(\lambda \frac{h^2}{a^2}\right)(1-\alpha)\left\{\sum_{m,n=1}^{N} \frac{mn(m^2+n^2)[(-1)^{m+n}-1]}{(m^2-n^2)^2} a_m a_n + \frac{\pi^2}{4}\sum_{m=1}^{N} m^2 a_m^2\right\}$$

$$+ \frac{\pi^2 k}{8}\left(\frac{h^2}{a^2}\right)\left(\lambda \frac{\mu}{M}\right)^{\frac{1}{2}}\left[\sum_{\substack{\ell,m,n=1 \\ |\ell-(m+n)|=k}}^{N} \frac{\ell m}{m+n} a_\ell \dot{a}_m a_n + \sum_{\substack{\ell,m,n=1 \\ |\ell-(m-n)|=k,\, m>n}}^{N} \frac{\ell a_\ell}{m-n}(n a_n \dot{a}_m - m \dot{a}_m a_n)\right.$$

$$\left. + \sum_{\substack{\ell,m,n=1 \\ \ell+m+n=k}}^{N} \frac{\ell m}{m+n} a_\ell \dot{a}_m a_n + \sum_{\substack{\ell,m,n=1 \\ \ell+m-n=k,\, m>n}}^{N} \frac{\ell a_\ell}{m-n}(n a_n \dot{a}_m - m \dot{a}_m a_n)\right]$$

$$+ \frac{\pi^2 k^2}{2}\left(\frac{h^2}{a^2}\right)\left(\lambda \frac{\mu}{M}\right)^{\frac{1}{2}}(1-\alpha) a_k \left(\sum_{m,n=1}^{N} \frac{mn(-1)^{m+n}}{m^2-n^2} \dot{a}_m a_n - \frac{1}{4}\sum_{m=1}^{N} \dot{a}_m a_m\right)$$

$$- \frac{\pi k}{2}\left(\frac{h^2}{a^2}\Delta p\right)\left\{\sum_{\ell,m=1}^{N} \frac{\ell m[1-(-1)^{k+\ell+m}]}{(k-\ell)^2-m^2} a_\ell a_m + \sum_{\ell,m=1}^{N} \frac{\ell m[1-(-1)^{k+\ell+m}]}{(k+\ell)^2-m^2} a_\ell a_m\right\}$$

(continued)

$$+ \frac{\pi k^2}{2} \left(\frac{h^2}{a^2} \Delta p \right) (1 - \alpha) a_k \sum_{n=1}^{N} \frac{1 - (-1)^n}{n} a_n$$

$$+ \frac{\pi^2 (\gamma + 1) k}{48} \lambda \left(M \frac{h}{a} \right)^2 \sum_{\ell, m, n=1}^{N} [1 - (-1)^{k+\ell+m+n}] \left\{ [k^2 - (\ell - m - n)^2]^{-1} + 2[k^2 - (\ell - m + n)^2]^{-1} \right.$$

$$\left. + [k^2 - (\ell + m + n)^2]^{-1} \right\} a_\ell a_m a_n = 0 \quad , \quad k = 1, 2, \ldots, N \tag{2.12}$$

With the exception of a slight difference in the definition of α , and the time-varying in-plane load R_0 , the terms up to and including the first appearance of Δp are the same as those derived by Dowell (Ref. 11): the von Kármán nonlinear structural operator for the panel, with linear piston-theory aerodynamic loading. The system parameters for this combination of terms are λ , μ/M , α , Δp , R_x , and R_0 . Furthermore, Dowell pointed out that these equations can be recast so as to eliminate the explicit appearance of α , so that only one (nonzero) value of α needs to be considered. With the addition of the nonlinear aerodynamic terms, the situation becomes more complicated. A new parameter, h/a , appears explicitly, and μ and M must be specified separately. Also, the explicit dependence on α can no longer be eliminated. The nonlinear aerodynamic terms appear in Eqs. (2.12) in the following order: first, those arising from the terms in $(F_z)_k$ dependent on $(\partial\bar{w}/\partial x)^2$, $(\partial\bar{w}/\partial x)$, $(\partial\bar{w}/\partial t)$, and $(\partial\bar{w}/\partial t)^2$, respectively; secondly, those arising from the terms in $(F_x)_0$ and $(F_x)_k$ dependent on $(\partial\bar{w}/\partial x)^2$, $(\partial\bar{w}/\partial x)$, $(\partial\bar{w}/\partial t)$, and $\overline{\Delta p}\ (\partial\bar{w}/\partial x)$, respectively; finally, those arising from the terms in $(F_z)_k$ dependent on $(\partial\bar{w}/\partial x)^3$. Note also that the panel geometric nonlinear terms are cubic in the a_k , whereas the nonlinear terms from $(F_z)_k$ are linear in h/a and quadratic in the a_k , and those from $(F_x)_0$ and $(F_x)_k$ are quadratic in h/a and cubic in the a_k .

For the complete equations, the functional dependence of the panel transverse displacement can be stated as

$$\bar{w}(x,t) = hFn\left[\frac{x}{a}, \tau ; \vec{A}_0 , \lambda , \mu , M , \frac{h}{a}, \alpha , \gamma , \Delta p , R_x , R_0\right] \qquad (2.13)$$

The method of solution is to integrate Eqs. (2.12) from given initial conditions $\vec{A}_0$ and to observe the resultant panel motion versus time. The use of piston theory, with its point-function relation between pressure and panel motion, makes this possible. The initial state-space vector $\vec{A}_0$ will not always govern the asymptotic behavior of $\bar{w}$; instances where this does occur will be discussed below. The computer program to integrate these equations was set up so as to allow individual nonlinear aerodynamic terms to be left out or included, as desired.

III. VERIFICATION; PRELIMINARY ASSESSMENT OF AERODYNAMIC NONLINEARITIES

3.1 Comparison with Previous Results

In order to check the numerical integration, a few test cases were run with linear aerodynamic loading, and the results were compared with those from Ref. 9. Figures 2 and 3 show the dimensionless panel displacement at the three-quarter chord vs. dimensionless time for values of system parameters noted on the figures. Figure 2 corresponds directly to Fig. 2 of Ref. 11, and the limit-cycle amplitude taken from Fig. 3 checks that given in Fig. 5 of Ref. 11. All the other test cases showed similar good agreement.

3.2 Behavior with Zero System Damping

Some interesting and unanticipated problems were encountered when the equations with linear aerodynamic loading were solved for zero system damping. Figures 4 and 5 show the panel response for the same set of initial conditions and system parameters used for Figs. 2 and 3, except that $\mu = 0$. After an initial transient shown in Fig. 4, the response becomes periodic but not simple harmonic, as is evidenced in Fig. 5. The response curve illustrated in Fig. 5 continues indefinitely without change, and the peak amplitude is different from that shown in Fig. 3. That the system does demonstrate instability for this set of parameters is illustrated in Fig. 6. Here the initial displacement at the three-quarter chord is smaller than that in Figs. 2-5 by a factor of approximately four, and the amplitude clearly grows with time. It then decreases, and the same process is repeated again (but is not shown here). Note also that the maximum amplitudes are different for the different initial conditions. This does not mean, however, that a unique limit-cycle amplitude and frequency are not associated with a given set of (supercritical) system parameters. In Fig. 7, the panel response is shown for $N = 2$ and for supercritical system parameters. The initial

conditions in this case were obtained from a harmonic-balance solution. It is seen that there is no initial transient, and the panel response continues at the same amplitude. Solutions for other values of system parameters exhibit the same behavior, and it can therefore be concluded that the method of calculating the panel motion with time will produce a limit cycle of constant amplitude for zero system damping only if the initial conditions correspond exactly to the limit-cycle modal amplitudes. For any other initial conditions, the panel oscillates between stable and unstable states. If, on the other hand, the system parameters are subcritical, the panel will oscillate without decaying, and the peak amplitude is determined by the initial conditions. Figures 8 and 9 show the panel displacement at the three-quarter chord for a subcritical value of λ and different initial conditions. Here it will be observed that the peak amplitudes never exceed the initial amplitudes, although the motion is not simple harmonic.

These results can also be interpreted with the aid of some general stability considerations for autonomous systems (Ref. 12). The panel equations for zero system damping describe a system whose state is uniquely determined by the $2N$ modal amplitudes and velocities a_k, $\dot{a}_k$, $k = 1,2,\ldots,N$, or in other words by a point in the 2N-dimensional space E_a^{2N}. The origin of this space is clearly an equilibrium point — it corresponds to the panel in a flat, undisturbed state — and it is desired to examine the stability of the panel in the neighborhood of this state. In brief, the origin is stable if for <u>any</u> sphere $S(R)$ of radius R in E_a^{2N}, centered on the origin, there exists another sphere $S(r)$ of radius $r \leq R$ such that any motion originating in $S(r)$ remains in $S(R)$ ever after. This stable behavior is exhibited in Figs. 8 and 9. Reducing the initial amplitude reduces the maximum resultant amplitude, so for any given bound on the amplitude the initial amplitude can be reduced to keep the resultant motion within the bound. On the other hand, if such a sphere $S(r)$ cannot be found, the origin is unstable. Figures 4, 5, and 6 illustrate this unstable situation. It is evident that there is an amplitude that the resultant motion will exceed, no matter how small

(but finite) the initial amplitude is. These same conclusions can be drawn when the initial conditions are broadened to include nonzero initial velocities, and the reader is referred to Ref. 12 for the full, precise definitions of stability and instability.

3.3 Isolated Effect of Aerodynamic Nonlinearities

The effects of aerodynamic nonlinearities were first considered by introducing into the equations of motion only the term from $(F_z)_k$ proportional to $(\partial\bar{w}/\partial x)^2$, with the in-plane restraint parameter α set to zero, so that no panel geometric nonlinear terms were present. For this single nonlinear aerodynamic term, only the new system parameter $M(h/a)$ is required. In Fig. 10, the panel is observed to be stable for $\lambda = 330$ and initial conditions given by $a_1(0) = -a_2(0) = 1.71$. In Fig. 11, the panel diverges with all system parameters unchanged and a slight increase in the initial deformation, to $a_1(0) = -a_2(0) = 1.72$. The divergence in this case is into the cavity, as expected, since an aerodynamic pressure proportional to $(\partial\bar{w}/\partial x)^2$ produces an increased pressure on the free-stream side of the panel for any panel displacement. Here, then, the asymptotic panel behavior is clearly governed by the initial conditions. On the other hand, with linear aerodynamic theory the panel would eventually return to its initial flat state, no matter what initial conditions would be given. (The classical linear critical value of λ for this case is approximately 343 – see Ref. 11, for example.)

IV. EFFECT OF AERODYNAMIC NONLINEARITIES ON POSTCRITICAL RESPONSE

Of interest here is how the aerodynamic nonlinear terms affect the motion and peak stress levels of the panel as it oscillates at a supercritical value of λ . Comparisons were made between the limit-cycle frequency and amplitude obtained with the nonlinear aerodynamic terms and those obtained with linear aerodynamic terms. Various combinations of system parameters, roughly characteristic of those found in practice, were tried. Various combinations of nonlinear aerodynamic terms were also tried, in an effort to identify those terms that would be important. It was soon found that for the system parameters surveyed only two had a significant effect — those resulting from terms in $(F_z)_k$ proportional to $(\partial\bar{w}/\partial x)^2$ and $(\partial\bar{w}/\partial x)\,(\partial\bar{w}/\partial t)$. With only these aerodynamic nonlinear terms in Eqs. (2.12), further simplification can be achieved through the transformation used by Dowell in Ref. 11. With $\tilde{a}_k = (\alpha)^{\frac{1}{2}}\, a_k$, $\tilde{R}_0 = (1-\alpha)\, R_0$, and $\tilde{\Delta}p = (\alpha)^{\frac{1}{2}}\, \Delta p$, the parameter α can be eliminated explicitly from the equations, and in addition to Dowell's parameters a single new one appears — $Mh/a(\alpha)^{\frac{1}{2}}$. This parameter then serves to measure the relative importance of nonlinear aerodynamic effects, since it ratios the principal factor governing the nonlinear aerodynamic terms to the one governing the panel geometric nonlinear terms. The functional dependence of the panel transverse displacement simplifies to

$$\bar{w}(x,t) = [h/(\alpha)^{\frac{1}{2}}]\; Fn[x/a\,,\ \tau\,;\ \vec{A}_0\,,\ \lambda\,,\ \mu/M\,,\ \gamma\,,\ Mh/a(\alpha)^{\frac{1}{2}}\,,\ \tilde{\Delta}p\,,\ R_x\,,\ \tilde{R}_0] \tag{4.1}$$

Postcritical panel response with linear aerodynamic loading was compared to that with nonlinear aerodynamic loading for various combinations of system parameters. A maximum value of 0.05 was taken for Mh/a (say, $h/a = 0.005$ and $M = 10.0$). A typical comparison is illustrated in Fig. 12, which compares the growth in peak limit-cycle amplitudes at $x/a = 0.75$ as a function of λ for linear and nonlinear aerodynamic

loading. Values of other system parameters are given in the caption. For the linear aerodynamic case, the panel oscillates as far into the airstream as it does into the cavity. With nonlinear aerodynamic loads, the peaks into the cavity (negative w) are greater, and those into the flow (positive w) are less. This effect is caused primarily by the nonlinear aerodynamic term dependent upon $(\partial\bar{w}/\partial x)^2$, which provides an overpressure, tending to push the panel into the cavity, as a result of any deviation of the panel from its flat initial position. However, any changes brought about by the nonlinear aerodynamic loading are quite small, even well into the supercritical regime, and the frequency of oscillation is virtually unchanged.

Since the in-plane restraint parameter α is the key parameter governing the influence of the panel geometric nonlinearity, one might expect that greater differences would be observed as α is reduced. A linear-nonlinear aerodynamic comparison is shown in Fig. 13 for $\lambda = 550$ and varying α . It can readily be observed that the nonlinear aerodynamic terms do have a relatively greater effect, to the extent that the peak displacement into the external flow at $x/a = 0.75$ is reduced some 23% for $\alpha = 0.1$. On the other hand, the corresponding peak displacement into the panel is increased by very little, and the frequency remains virtually unaffected.

Another important consideration is the change in stress caused by nonlinear aerodynamic loading. The stress in the panel can be written in terms of modal amplitudes and other system parameters as (Ref. 11)

$$\sigma_x = \frac{1-\nu^2}{E(h/a)^2}\bar{\sigma}_x = \frac{z}{h}\sum_{k=1}^{N}(k\pi)^2 a_k \sin\frac{k\pi x}{a} + \frac{R_x + (1-\alpha)R_0}{12} + \frac{\alpha}{4}\sum_{k=1}^{N}(k\pi a_k)^2 \qquad (4.2)$$

The maximum or minimum of σ_x at any instant of time occurs for $z = \pm h/2$, so it is seen that the stress distributions for maximum

and minimum stress will plot as curves symmetric about a mean, the stress due to stretching, given by the constant terms in Eq. (4.2). Figure 14 compares these stress distributions in the panel, at the instant the displacement at $x/a = 0.75$ reaches a peak, for $\alpha = 0.1$ and $\lambda = 550$. The maximum tensile and compressive stresses occur at $x/a \simeq 0.85$, and the nonlinear aerodynamic loading increases these stresses by at most 5%. For aluminum, $E \simeq 10^7$ psi and $\nu = 1/3$; with $h/a = 0.005$, a stress σ_x of 60 corresponds to a dimensional stress $\bar{\sigma}_x$ of 16,900 psi, which is well below the yield stresses of approximately 60,000 psi in tension and 40,000 psi in compression. Convergence studies on stress by Dowell (Ref. 9) indicate that six modes $(N = 6)$ may not be adequate for stresses, although this number is satisfactory for displacements. However, it is not felt that using enough modes to converge the stresses would alter the conclusion that the assumption of stress levels within the linear range is a valid one.

Another key assumption in the derivation of the panel equations of motion is that $(\partial\bar{w}/\partial x)^2$ is everywhere much less than unity. In terms of modal amplitudes, this is

$$\left(\frac{\partial \bar{w}}{\partial x}\right)^2 = \left(\frac{h}{a}\right)^2 \left(\sum_{k=1}^{N} k\pi a_k \cos\frac{k\pi x}{a}\right)^2 \qquad (4.3)$$

This distribution was calculated for various large-amplitude panel states. Generally, the largest values were at $x = a$, and the largest of these calculated was approximately 0.01, which was calculated from the mode shape corresponding to the nonlinear-aerodynamic stress distribution of Fig. 14. Values calculated for other cases and over other portions of the panel were much smaller, thereby strongly suggesting that the "moderate-rotation" assumption is also justified.

One final check involved testing the accuracy of the numerical integration. This was done by integrating the equations of motion backward in time, with initial conditions given by the state of the panel at some instant during a previous calculation. Panel motions with time could

then be compared. The parameter in the numerical-integration subroutine governing acceptable relative error between integration steps was kept small enough so that no appreciable differences arose between forward and backward integrations over the longest time intervals contemplated.

The results presented in this section are representative of the responses calculated for a variety of conditions. From this evidence, it can be concluded that the influence on postcritical response of nonlinear aerodynamic loading, of the type considered herein, is minor. The postcritical motion is generally such that the aerodynamic terms quadratic in $\partial\bar{w}/\partial x$ do very little net work over a cycle, and the cubic terms, which would do work over a cycle, are not important unless Mh/a is unrealistically large. It was observed, however, that transient motions — such as those that were calculated before steady-state amplitude and frequency were attained — were affected markedly by the nonlinear aerodynamic terms. It is therefore entirely possible that these terms would be very important when panel transient response is studied at hypersonic speeds. The two nonlinear aerodynamic terms used in this section were the only ones retained for subsequent studies, except for occasional check runs to ensure that other terms were not contributing significantly to the results.

V. EFFECT OF AERODYNAMIC NONLINEARITIES ON STABILITY

5.1 Comparison with Experiment

As a first step towards reproducing the experimental conditions of Ref. 1, as discussed in Sec. I, it was decided to study the panel response as the in-plane applied load was varied across the linear stability boundary. This involves scheduling the time-varying load R_0 with time; a typical case is shown in Fig. 15. The panel was initially set in motion at point A, on the stable side of the linear stability boundary. Then the in-plane load was decreased to point B, on the unstable side, and held there until the motion of the panel was established. Finally, the load was increased to point A, where the nonlinear aerodynamic terms dictate the resultant stability characteristics. Figure 16 presents a time history of the displacement at $x/a = 0.75$ for values of λ and in-plane load corresponding to point A in Fig. 15. The motion shown is that which results after the in-plane load has been cycled from point A to point B and back to point A. Figure 16 shows that the energy imparted to the panel while the load is at point B is enough to cause instability with the load at point A. To stabilize the panel, it would be necessary to increase the load even more.

The scenario described above is consistent with the experimental observations of Ref. 1, but the parameters used were not comparable. The next step was then to attempt a closer comparison by looking for an amplitude-sensitive instability with parameters corresponding to the experimental conditions. The following parameters were chosen: $R_x = 160$, $\lambda = 2000$, $M = 10$, $\mu = 0.1$, $\Delta p = 0$, and $h/a = 0.00054$. These values give a condition that is just on the stable side of the linear stability boundary for a panel on hinged supports. Experimental edge conditions would be better represented with clamped supports, but the theoretical differences between stability boundaries for these two edge conditions

are not really significant when the in-plane applied loads are as large as they were in the experiments (see Ref. 1). The remaining unknown parameter is α . Various initial amplitudes were used, appropriate to flutter amplitudes observed experimentally ($w \simeq 10$ in some cases), and α was varied in order to see if these initial amplitudes would produce an unstable panel motion. The only unstable motion that could be produced was an oscillatory but divergent one, for values of α on the order of 10^{-3}. These results indicate that nonlinear aerodynamic influences are not the cause of the experimentally observed behavior, since the value of α needed and the corresponding calculated unstable motion are not consistent with the experimental setup or observations.

5.2 Constant-Initial-Energy Stability Boundary

After it was demonstrated that energy levels capable of causing amplitude-sensitive instability could be generated by unstable panel motion near the linear stability boundary, it was decided to consider how the linear stability boundary — presented, say, in the $\lambda - R_x$ plane with other parameters fixed — would be changed for a given level of initial excitation.

Portraying analytically the dependence of the amplitude-sensitive instability on $\vec{A}_0$ would be a formidable, if not impossible, task, since it has $2N$ elements. One simplified approach is suggested by the work of Dimantha and Roorda (Ref. 13). They investigate the stability of nonlinear nonconservative systems with the direct method of Liapunov, with Zubov's procedure for constructing the Liapunov functional. It is not at all clear whether this method is applicable to the panel stability problem; however, the ideas in Ref. 13 do at least suggest a meaningful procedure for the numerical experimentation described in this report. In principle, one can determine a stability boundary for the panel in terms of the elements of $\vec{A}_0$ for fixed system parameters. This boundary can be viewed as a hypersurface S in the phase space determined by the elements of $\vec{A}_0$. (Note that the origin of this phase space represents the panel in its flat undisturbed equilibrium position.) Any combination

of initial conditions that plots on one side of S will result in unstable panel motion, while a combination that plots on the other side will result in stable motion. Dimantha and Roorda proposed to calculate the minimum total panel energy on S , such that this minimum value E_1 will determine a hypersphere that just touches S at one or more points and is everywhere else on the stable side of S . The energy E_1 then provides an upper bound for the initial disturbance energy such that the resultant panel motion is stable. In similar fashion, Dimantha and Roorda also proposed to determine the maximum total energy on S , thereby determining a hypersphere of energy level E_2 that gives a lower bound on the initial disturbance energy for unstable motion. The reader is referred to Ref. 13 for the full details of this analysis. It suffices to say here that these ideas suggest determining a nonlinear stability boundary in the $\lambda - R_x$ plane for constant initial energy and comparing this boundary with the linear stability boundary, which is independent of the initial conditions.

The dimensionless panel energy is given by (Ref. 10):

$$E' = \frac{a^3}{Dh^2}\bar{E} = \frac{1}{4}\sum_{k=1}^{N}\dot{a}_k^2 + \frac{3\pi^4}{8}\alpha\sum_{k,\ell=1}^{N}k^2\ell^2 a_k^2 a_\ell^2$$

$$+ \frac{\pi^2}{4}R_x\sum_{k=1}^{N}k^2 a_k^2 + \frac{\pi^4}{4}\sum_{k=1}^{N}k^4 a_k^2 \qquad (5.1)$$

Note that the time-varying applied load, R_0 , is here set to zero. The initial choice of energy level was that corresponding to supercritical panel motion near the linear $\lambda - R_x$ stability boundary. It was further decided, purely arbitrarily, to set $a_1(0) = -a_2(0)$ and to let these be the only nonzero components of $\vec{A}_0$. With $E_0 = 1750$ and $\alpha = 0.1$, the variation of $a_1(0) = -a_2(0)$ with R_x is given in Fig. 17.

The remaining system parameters were then chosen, and a new stability boundary was determined, as is shown in Fig. 18. This boundary was obtained by integrating the panel equations of motion, with initial

conditions determined as discussed above, and observing whether or not the calculated panel motion persisted or died out past the initial transient. The complicated nature of the dependence of this stability boundary on the initial energy (and, ultimately, on $\vec{A}_0$) can be inferred from the shape of the boundary. As noted in Ref. 5, the onset of the instability over virtually the whole boundary is characterized by a strong traveling-wave component, quite similar to the "periodic but non-simple-harmonic" behavior noted by Dowell (Ref. 11) for large compressive values of R_x with linear aerodynamic loading. Observe also that the maximum reduction in stability occurs for zero or slightly positive (tensile) values of R_x . The behavior of the nonlinear stability boundary near $R_x = -0.5\,\pi^2$ has not been explained.

5.3 Parametric Survey

The procedure of the previous subsection was then used to determine unstable regions with variations in other system parameters. Figure 19 gives the variation of the value of λ where instability first occurs with both different energy levels and different modal content. For $E_0 = 1750$, there are only minor differences in the critical value of λ among the three sets of nonzero elements of $\vec{A}_0$ that were examined. Almost tripling the initial energy for one of these sets produced little change in the critical value of λ . For $E_0 = 3500$, there is an unstable band bounded by stable regions, suggesting the same sort of contortions in the stability boundary near $R_x = 0$ as was observed in Fig. 18 near $R_x = -0.5\,\pi^2$.

Figure 20 presents the effects of both positive and negative static pressure differences for $R_x = 0$ and the initial conditions of Fig. 18. Negative values of Δp produce a static pressure tending to push the panel into the cavity, reinforcing the deformation caused by the aerodynamic term proportional to $(\partial\bar{w}/\partial x)^2$ and slightly adding to its destabilizing influence. Just the opposite occurs for positive values of Δp .

As would be expected, the parameter $Mh/a(\alpha)^{\frac{1}{2}}$ has a strong influence on the amplitude-sensitive instability, as is shown in Fig. 21. Increasing values of $Mh/a(\alpha)^{\frac{1}{2}}$, which represent increased relative importance of the nonlinear aerodynamic terms, result in monotonically decreasing critical values of λ. The slopes of these curves at the λ axis give a measure of the importance of nonlinear aerodynamic effects. Generally, they should all be zero for zero initial energy and decrease as the initial energy increases, but the results in Fig. 19 suggest a complicated picture, and any unsupported generalization must be viewed with caution.

VI. A NEW METHOD OF ANALYSIS

6.1 Kamel's Perturbation Method

Although it produces a great amount of information, direct integration of the equations of motion has certain disadvantages. The information produced is essentially similar to that produced experimentally, and the analyst is forced to conduct a number of "numerical experiments" in order to determine the influence of the system parameters on the panel's behavior. Clearly, it would be extremely worthwhile to have a method of analysis that would permit the direct analytical determination of the information desired. For example, such a method would be very useful in calculating an amplitude-sensitive stability boundary, such as the one given in Fig. 18. What is desired, then, is an approximate method that is capable of displaying analytically the influence of such parameters as $\vec{A}_0$ or Mh/a on this stability boundary. The perturbation method of Kamel (Ref. 14), which was independently developed at Stanford concurrently with the present work, appeared to be a likely candidate. A brief description of this method follows; the reader is referred to Ref. 14 for more details.

Consider a given system of ordinary differential equations written in the following form:

$$\dot{\vec{c}}(\tau;\epsilon) = \vec{g}(\vec{c},\tau;\epsilon) = \sum_{k=0}^{\infty} \frac{\epsilon^k}{k!} \vec{g}^{(k)}(\vec{c},\tau) \qquad (6.1)$$

Here ϵ is a small parameter, and $\vec{g}$ is assumed to depend analytically on ϵ, so that the Taylor-series expansion of Eq. (6.1) is valid. The idea underlying Kamel's method is to transform the dependent variable $\vec{c}(\tau)$ to a new set, $\vec{\bar{c}}(\tau)$, such that the transformed equations governing this new set have certain characteristics. For example, to investigate stability the analyst is interested in the asymptotic behavior of $\vec{c}(\tau)$.

He would therefore construct the transformation so that the new dependent variables display only the secular, or long-period, behavior of the system. By doing so, the analyst presumably also comes up with a much simpler set of equations that he can solve analytically. This transformation is of the form

$$\vec{\vec{c}}(\tau;\epsilon) = \vec{c}(\tau) + \sum_{k=1}^{\infty} \frac{\epsilon^k}{k!} \vec{c}^{(k)}(\vec{c},\tau) \tag{6.2}$$

such that $\vec{\vec{c}}(\tau)$ satisfies

$$\frac{d\vec{\vec{c}}}{d\epsilon} = \vec{W}(\vec{\vec{c}},\tau;\epsilon) = \sum_{k=0}^{\infty} \frac{\epsilon^k}{k!} \vec{W}_{k+1}(\vec{\vec{c}},\tau) \tag{6.3}$$

for the initial conditions

$$\vec{\vec{c}}(\tau;0) = \vec{c} \tag{6.4}$$

The functions $\vec{W}_k$ are to be determined from the requirement that the transformed differential equations

$$\dot{\vec{\vec{c}}}(\tau;\epsilon) = \vec{f}(\vec{\vec{c}},\tau;\epsilon) = \sum_{k=0}^{\infty} \frac{\epsilon^k}{k!} \vec{f}_k(\vec{\vec{c}},\tau) \tag{6.5}$$

contain only secular or long-period terms. The $\vec{f}_n$ are obtained by eliminating these same terms from the governing differential equations for the $\vec{W}_k$:

$$\frac{\partial \vec{W}_k}{\partial \tau} = \vec{f}_k - \vec{g}^{(k)} + \sum_{\ell=1}^{k-1} \left(C_{\ell-1}^{k-1} L_\ell \vec{f}_{k-\ell} - C_\ell^{k-1} \vec{g}_{\ell,k-\ell} \right) , \quad k = 1,2,\ldots \tag{6.6}$$

where

$$\left.\begin{aligned} \vec{g}'_{k,\ell} &= -\sum_{m=1}^{k} C_{m-1}^{k-1} L_m \vec{g}'_{k-m,\ell} \\ L_k \vec{F} &= \frac{\partial \vec{F}}{\partial \vec{c}} \vec{W}_k - \frac{\partial \vec{W}_k}{\partial \vec{c}} \vec{F} \\ C_k^{\ell} &= \frac{\ell!}{k!(\ell-k)!} \quad , \quad \vec{g}'_{0,k} = g^{(k)} \end{aligned}\right\} \tag{6.7}$$

Equations (6.6) and (6.7) form recursive relations for obtaining $\vec{W}_k$ and $\vec{f}_k$, since all other functions in these equations can be constructed from known quantities. This ability to obtain higher-order approximations recursively is one of the principal advantages of Kamel's method.

With $\vec{W}_k$ and $\vec{f}_k$ calculated to any order desired, the original dependent variables $\vec{c}$ can be found in terms of $\vec{\vec{c}}$ in the form

$$\vec{c} = \vec{\vec{c}} + \sum_{k=1}^{\infty} \frac{\epsilon^k}{k!} \vec{\vec{c}}_n(\vec{\vec{c}}) \tag{6.8}$$

A recursive formula for the $\vec{\vec{c}}_k$ is

$$\vec{\vec{c}}_k(\vec{\vec{c}}) = -\vec{W}_k(\vec{\vec{c}}) - \sum_{\ell=1}^{k-1} C_{\ell-1}^{k-1} \vec{c}_{\ell,k-\ell}(\vec{\vec{c}}) \tag{6.9}$$

with

$$\vec{c}_{k,\ell} = -\sum_{m=1}^{k} C_{m-1}^{k-1} L_m \vec{c}_{k-m,\ell}(\vec{\vec{c}}) \qquad \text{(continued)}$$

and

$$L_k \vec{F} = \frac{\partial \vec{F}}{\partial \vec{c}} \vec{W}_k \quad , \quad \vec{c}_{0,k} = \vec{c}^{(k)} \tag{6.10}$$

In summary, then, Kamel's algorithm proceeds by determining the $\vec{W}_k$ and $\vec{f}_k$ from Eqs. (6.6) and (6.7), to whatever order is desired. The $\vec{f}_k$ are chosen so as to cancel secular terms from Eqs. (6.6). These $\vec{f}_k$, in turn, give the differential equations for the transformed dependent variables, from Eqs. (6.5). These equations are integrated, and Eqs. (6.8)-(6.10) are used to determine the long-period behavior of the system. This method is similar in spirit to the method of multiple time scales, as applied by Morino (Ref. 15) to panel flutter.

6.2 Example — Two Modes

To illustrate the application of Kamel's method, let us consider a two-mode version of Eqs. (2.12), with $R_0 = 0$, $\Delta p = 0$, and the two nonlinear aerodynamic terms that were previously found to be the most important — those proportional to $(\partial \bar{w}/\partial x)^2$ and $(\partial \bar{w}/\partial x)(\partial \bar{w}/\partial t)$. In addition, let $\tilde{\tau} = \tau(\lambda)^{\frac{1}{2}}$, $\tilde{a}_k = a_k(\alpha)^{\frac{1}{2}}$, and define

$$\left.\begin{aligned} \epsilon_1 &= \frac{\lambda - \lambda_c}{\lambda} \\ \left(1 + \frac{R_x}{\pi^2}\right)(1 - \epsilon_1) &= 1 + \epsilon_2 \end{aligned}\right\} \tag{6.11}$$

Here allowance is being made for small perturbations from $\lambda = \lambda_c$ and from $R_x = 0$, so that λ_c is the critical value of λ for the linear theory with no in-plane loading. If substantial values of R_x are required, then R_x/π^2 can be treated as another fixed system parameter, and terms involving it can be left with the other linear terms. With

these scalings, Eqs. (2.12) can be written for two modes as

$$\ddot{\tilde{a}}_1 + \left(\frac{\mu}{M}\right)^{\frac{1}{2}} \dot{\tilde{a}}_1 + \frac{\pi^4}{\lambda_c}\tilde{a}_1 - \frac{8}{3}\tilde{a}_2 = -\frac{\pi^4}{\lambda_c}\epsilon_2\tilde{a}_1$$

$$- \frac{(\gamma+1)\pi}{3} \frac{Mh}{a(\alpha)^{\frac{1}{2}}} \left(\tilde{a}_1^2 + \frac{28}{5}\tilde{a}_2^2\right)$$

$$- \frac{(\gamma+1)\pi}{4} \left(\frac{\mu}{M}\right)^{\frac{1}{2}} \frac{Mh}{a(\alpha)^{\frac{1}{2}}} (\tilde{a}_1\dot{\tilde{a}}_2 - 2\dot{\tilde{a}}_2\tilde{a}_1) - \frac{3\pi^4}{\lambda_c}\tilde{a}_1(\tilde{a}_1^2 + 4\tilde{a}_2^2)$$

$$= Q_1 + C_1 \qquad (6.12)$$

$$\ddot{\tilde{a}}_2 + \left(\frac{\mu}{M}\right)^{\frac{1}{2}} \dot{\tilde{a}}_2 + \frac{16\pi^4}{\lambda_c}\tilde{a}_2 + \frac{8}{3}\tilde{a}_1 = -\frac{4\pi^4}{\lambda_c}(\epsilon_2 - 3\epsilon_1)\tilde{a}_2$$

$$- \frac{8\pi(\gamma+1)}{15} \frac{Mh}{a(\alpha)^{\frac{1}{2}}}\tilde{a}_1\tilde{a}_2 - \frac{(\gamma+1)\pi}{4}\left(\frac{\mu}{M}\right)^{\frac{1}{2}} \frac{Mh}{a(\alpha)^{\frac{1}{2}}}\tilde{a}_1\dot{\tilde{a}}_2$$

$$- \frac{12\pi^4}{\lambda_c}\tilde{a}_2(\tilde{a}_1 + 4\tilde{a}_2^2)$$

$$= Q_2 + C_2$$

Note that the dot superscript here denotes differentiation with respect to $\tilde{\tau}$ rather than τ ; this notation is restricted to this Section.

The equations have been arranged so that all nonlinear terms are on the right-hand sides. With the presumption that $\tilde{a}_k = O(\epsilon_1)$, these terms are arranged as quadratic (Q_k) and cubic (C_k) terms. For

$\mu/M = 0.01$, the characteristic equation of the linear system produces $\lambda_c = 274.545$, and four roots σ_k and eigenvectors $\vec{U}_k = (1, U_{k,2})$, arranged in complex conjugate pairs as follows:

$$\sigma_1 = 1.736608\ i$$

$$\sigma_2 = -0.10 + 1.736606\ i$$

$$\sigma_3 = -1.736608\ i$$

$$\sigma_4 = -0.10 - 1.736606\ i$$

$$U_{12} = -0.9978764 + 0.0651227\ i$$

$$U_{22} = -0.9978751 - 0.0651227\ i$$

$$U_{32} = -0.9978764 - 0.0651227\ i$$

$$U_{42} = -0.9978751 + 0.0651227\ i$$

Since the nonlinear terms in Eqs. (6.12) contain time derivatives, the equations must be manipulated so as to put them in a form suitable for the application of Kamel's method. This is accomplished by variation of parameters. With $\vec{a} = (\tilde{a}_1, \tilde{a}_2)$, let

$$\vec{a}(\tilde{\tau}) = \sum_{k=1}^{4} c_k(\tilde{\tau})\, e^{\sigma_k \tilde{\tau}}\, \vec{U}_k \qquad (6.13)$$

It is then required that

$$\dot{\vec{a}} = \sum_{k=1}^{4} c_k \sigma_k\, e^{\sigma_k \tilde{\tau}}\, \vec{U}_k \qquad (6.14)$$

which implies

$$\sum_{k=1}^{4} \dot{c}_k \, e^{\sigma_k \tilde{\tau}} \, \vec{U}_k = 0 \tag{6.15}$$

Substituting for the a_k in terms of the c_k in Eqs. (6.12) yields

$$\sum_{k=1}^{4} \dot{c}_k \sigma_k \, e^{\sigma_k \tilde{\tau}} \, \vec{U}_k = \vec{F} = (Q_1 + C_1 \, , \, Q_2 + C_2) \tag{6.16}$$

Equations (6.15) and (6.16) constitute four equations in the four new dependent variables $c_k(\tilde{\tau})$; note that $\dot{c}_k$ does not appear in either the Q_k or the C_k , since from Eqs. (6.14) the $\dot{a}_k$ depend only on the c_k . Equations (6.15) and (6.16) can now be inverted to give a set of equations in the desired form:

$$\dot{c}_k = e^{-\sigma_k \tilde{\tau}} \left([B]\{G\} \right)_k = g_k^{(1)} + g_k^{(2)} + \ldots \tag{6.17}$$

The matrix $[B]$ is a 4×4 matrix whose inverse is

$$[B]^{-1} = \begin{bmatrix} 1 & 1 & 1 & 1 \\ U_{12} & U_{22} & U_{32} & U_{42} \\ \sigma_1 & \sigma_2 & \sigma_3 & \sigma_4 \\ \sigma_1 U_{12} & \sigma_2 U_{22} & \sigma_3 U_{32} & \sigma_4 U_{42} \end{bmatrix} \tag{6.18}$$

and $\{G\}$ is a 4×1 column matrix

$$\{G\}^T = \begin{bmatrix} 0 & 0 & Q_1 + C_1 & Q_2 + C_2 \end{bmatrix} \tag{6.19}$$

For example,

$$g_1^{(1)} = e^{-\sigma_1 \tilde{\tau}} \left\{ B_{13} \left(-\frac{\pi^4}{\lambda_c} \epsilon_2 \sum_{k=1}^{4} c_k e^{\sigma_k \tilde{\tau}} + Q_1' \right) + B_{14} \left[-\frac{4\pi^4}{\lambda_c} (\epsilon_2 - 3\epsilon_1) \sum_{k=1}^{4} c_k U_{k,2} e^{\sigma_k \tilde{\tau}} + Q_2' \right] \right\} \qquad (6.20)$$

Here Q_k' is used to denote that portion of Q_k that is quadratic in the a_k and therefore quadratic in the c_k .

Clearly, Eqs. (6.17) cannot be integrated in closed form, although presumably they could be integrated numerically. A transformed set of dependent variables is now sought that will exhibit the asymptotic behavior of the panel:

$$\dot{\bar{c}}_k = f_{1,k} + f_{2,k} + \cdots \qquad (6.21)$$

The first step is to go to Eqs. (6.6) for $k = 1$. A typical equation that results is

$$\frac{\partial W_{11}}{\partial \tilde{\tau}} = f_{11} - g_1^{(1)} \qquad (6.22)$$

where $g_1^{(1)}$ is now written in terms of the $\bar{c}_k$ rather than the c_k . The function f_{11} is to be chosen so as to eliminate secular terms from Eq. (6.22). Examination of Eq. (6.20) shows that such terms will come about only where $k = 1$ in the two summations, as a result of cancellation of the exponentials. With the values of the σ_k being either pure imaginary or complex with negative real parts, there are no other

terms in Eq. (6.20) that could produce asymptotic instability. Hence,

$$f_{11} = \left[- B_{13} \frac{\pi^4}{\lambda_c} \epsilon_2 - B_{14} \frac{4\pi^4}{\lambda_c} (\epsilon_2 - 3\epsilon_1) U_{12} \right] \bar{c}_1 \qquad (6.23)$$

and similar reasoning for W_{12} gives

$$f_{12} = \left[- B_{23} \frac{\pi^4}{\lambda_c} \epsilon_2 - B_{24} \frac{4\pi^4}{\lambda_c} (\epsilon_2 - 3\epsilon_1) U_{22} \right] \bar{c}_2 \qquad (6.24)$$

For $k = 1$, Eqs. (6.6) then become

$$\frac{\partial W_{1,\ell}}{\partial \tilde{\tau}} = e^{-\sigma_\ell \tilde{\tau}} \left\{ B_{\ell,3} \left(\frac{\pi^4}{\lambda_c} \epsilon_2 \sum_{\substack{k=1 \\ k \neq \ell}}^{4} \bar{c}_k e^{\sigma_k \tilde{\tau}} - Q_1' \right) + B_{\ell,4} \left[\frac{4\pi^4}{\lambda_c} (\epsilon_2 - 3\epsilon_1) \sum_{\substack{k=1 \\ k \neq \ell}}^{4} \bar{c}_k U_{2,k} e^{\sigma_k \tilde{\tau}} - Q_2' \right] \right\} , \quad \ell = 1,2 \qquad (6.25)$$

These equations are integrated to give the $W_{1,\ell}$ for input to Eqs. (6.6) with $k = 2$, and f_{21} and f_{22} are chosen to eliminate any secular terms. Cubic terms ($g_1^{(2)}$ and $g_2^{(2)}$) are involved, and the algebra becomes formidable, so it will not be repeated here. (It was, in fact, performed on the computer.) The type of secular term that is found is illustrated by the form chosen for f_{21} :

$$f_{21} = D_2 |\bar{c}_1^2| \bar{c}_1 \qquad (6.26)$$

The parameter D_2 is a complex constant depending in a complicated manner upon the system parameters and the elements of the matrix [B] . For the panel problem, this second pass through the algorithm is all

that is needed, and the differential equation for $\bar{c}_1$ can be written as

$$\dot{\bar{c}}_1 = f_{11} + f_{21} = D_1\bar{c}_1 + D_2|\bar{c}_1^2|\bar{c}_1 \tag{6.27}$$

Note that D_1 is used to represent the coefficient of $\bar{c}_1$ given in Eq. (6.23). Equation (6.27) has the solution

$$\bar{c}_1 = \bar{c}_{1,0}\left[1 - \frac{D_{2R}\bar{c}_{1,0}^2}{D_{1R}}\left(e^{2D_{1R}\tilde{\tau}} - 1\right)\right]^{-\frac{1}{2}} e^{D_1\tilde{\tau} + i\theta_1} \tag{6.28}$$

where D_{kR} is the real part of D_k and $\bar{c}_{1,0}$ is the initial magnitude of $\bar{c}_1$, $|\bar{c}_1(0)|$. The phase angle $\theta_1(\tilde{\tau})$ is given by $(\theta_{1,0} = \theta_1(0))$

$$\theta_1 = \theta_{1,0} - \frac{D_{2I}}{2D_{2R}\bar{c}_{1,0}} \ln\left|1 - \frac{D_{2R}\bar{c}_{1,0}^2}{D_{1R}}\left(e^{2D_{1R}\tilde{\tau}} - 1\right)\right| \tag{6.29}$$

It can already be seen that one important goal has been reached, in that the dependence of the asymptotic behavior of the panel on the initial conditions is explicitly displayed in Eq. (6.28).

Equations (6.8)-(6.10) are now utilized to construct the $c_k(\tilde{\tau})$, from which the $a_k(\tilde{\tau})$ can be found from Eqs. (6.13). For the c_k, we find

$$c_k(\tilde{\tau}) = \bar{c}_k(\tilde{\tau}) - W_{1,k}(\bar{c}_k,\tilde{\tau}) - W_{2,k}(\bar{c}_k,\tilde{\tau}) - \frac{\partial W_{1,k}(\bar{c}_k,\tilde{\tau})}{\partial \bar{c}_k} W_{1,k}(\bar{c}_k,\tilde{\tau}) \quad , \quad k = 1,2,3,4 \tag{6.30}$$

It is not necessary, however, to calculate all of the terms in these equations, if stability is of interest. All that is necessary is to

examine the secular terms, which are contained in $\bar{c}_k(\tilde{\tau})$. This fact, coupled with the requirement that the transformations of Eqs. (6.13) produce real $\tilde{a}_k$ from complex c_k , σ_k , and $\vec{U}_k$, permits the asymptotic behavior of the system to be examined very easily. For example, the asymptotic behavior of $\tilde{a}_1$ is given by

$$\tilde{a}_1(\tilde{\tau}) \sim 2\mathrm{Re}\left(\bar{c}_1 e^{\sigma_1\tilde{\tau}} U_{11}\right) = 2\mathrm{Re}\left(\bar{c}_1 e^{\sigma_1\tilde{\tau}}\right) \tag{6.31}$$

Using Eq. (6.28) gives

$$\tilde{a}_1(\tilde{\tau}) \sim 2\bar{c}_{1,0} e^{D_{1R}\tilde{\tau}} \left[1 - \frac{D_{2R}\bar{c}_{1,0}^2}{D_{1R}}\left(e^{2D_{1R}\tilde{\tau}} - 1\right)\right]^{-\frac{1}{2}} \cos\left(\omega_1\tilde{\tau} + D_{1I}\tilde{\tau} + \theta_1\right) \tag{6.32}$$

with $\omega_1 = |\sigma_1|$. This equation can be manipulated to give

$$\tilde{a}_1(\tilde{\tau}) \sim 2\left[\frac{D_R}{\left(1 + \frac{D_R}{\bar{c}_{1,0}^2}\right)e^{-2D_{1R}\tilde{\tau}} - 1}\right]^{\frac{1}{2}} \cos\left(\omega_1\tilde{\tau} + D_{1I}\tilde{\tau} + \theta_1\right) \tag{6.33}$$

where $D_R = D_{1R}/D_{2R}$. The initial amplitude $\bar{c}_{1,0}$ is seen to be one half of $\tilde{a}_1(0)$. The parameter D_1 is linear in ϵ_1 and ϵ_2 , while D_2 does not depend on ϵ_1 or ϵ_2 , so it can easily be shown that $\tilde{a}_1$ can be expanded in a power series in ϵ_1 , as was assumed initially (ϵ_2 is assumed $O(\epsilon_1)$) . The parameter $Mh/a(\alpha)^{\frac{1}{2}}$, which is the principal parameter governing the amplitude-sensitive instability, influences only D_2 .

The stability characteristics can be evaluated by examining the amplitude term in Eq. (6.33). A number of cases can be distinguished:

I. $D_R < 0$:

For $\tilde{\tau} = 0$, both numerator and denominator are negative, so the ratio is positive. If $\bar{c}_{1,0}^{-2} = - D_R$, then a limit cycle of constant amplitude $2\bar{c}_{1,0}$ is obtained, regardless of the sign of D_{1R} .

A. $D_{1R} < 0$:

If $\bar{c}_{1,0}^{-2} < |D_R|$, there is a limit cycle whose amplitude approaches $2\bar{c}_{1,0}$ as $\tilde{\tau}$ approaches infinity. If $\bar{c}_{1,0}^{-2} > |D_R|$, then there is a divergent instability at a finite time

$$\tilde{\tau}_D = - \frac{\ln \left(1 + \frac{D_R}{\bar{c}_{1,0}^{-2}} \right)}{2D_{1R}}$$

B. $D_{1R} > 0$:

There is a limit cycle whose amplitude approaches $(- D_R)^{\frac{1}{2}}$, independently of the magnitude of $\bar{c}_{1,0}^{-2}$.

II. $D_R > 0$:

For $\tilde{\tau} = 0$, both numerator and denominator are positive.

A. $D_{1R} < 0$:

Stability is indicated, since $\tilde{a}_1 \to 0$ as $\tilde{\tau} \to \infty$.

B. $D_{1R} > 0$:

There is a divergent instability at

$$\tilde{\tau}_D = \frac{\ln \left(1 + \frac{D_R}{\bar{c}_{1,0}^{-2}} \right)}{2D_{1R}}$$

Note that D_1 will change sign, since it is proportional to ϵ_1, which changes sign as λ goes through λ_c.

For a numerical example, let $R_x = 0$, so that $\epsilon_2 = -\epsilon_1$. With $Mh/a(\alpha)^{\frac{1}{2}} = 0.158$, we find

$$D_1 = (11.76 - 0.5300\ i)\ \epsilon_1\ ,\quad D_2 = -6.563 - 1.404\ i$$

For $\lambda < \lambda_c$, $\epsilon_1 < 0$, so this is case IIA. The panel is stable; no amplitude-sensitive instability can occur. The sign of D_{1I} indicates an increase in frequency. For $\lambda > \lambda_c$, $\epsilon_1 > 0$, and case IB is applicable -- there is a limit cycle whose amplitude is independent of $\bar{c}_{1,0}$, and the frequency is reduced from its value at $\lambda = \lambda_c$. (Note that the special case $\bar{c}_{1,0}^2 = |D_R|$ does not alter this conclusion.)

Although this numerical example did not produce an amplitude-sensitive instability, there are parameter regions where such an instability will be found. The conclusions reached above are consistent with physical intuition, in that the changes in frequency and the character of the supercritical limit cycle are what would be expected in the absence of amplitude-sensitive instability.

VII. CONCLUDING REMARKS

It has been shown theoretically that, under proper conditions, nonlinear aerodynamic loading can produce unstable panel motion in a parameter region that would be a stable one on the basis of a model with linear aerodynamics. The principal factors in determining the likelihood of such an instability are the excitation level that the panel is expected to encounter and the importance of the nonlinear aerodynamic loading in comparison with the stabilizing effect of in-plane stretching in the panel. The latter factor is measured directly by the interaction parameter $Mh/a(\alpha)^{\frac{1}{2}}$. For a given initial excitation, the critical value of λ varies quite smoothly with this parameter. On the other hand, the dependence of the instability on the nature of the initial conditions is quite complicated. This particular conclusion should not be too surprising, since the system itself is far from simple.

To the best of the author's knowledge, amplitude-sensitive flutter has not been observed experimentally, at least for flat or slightly curved panels. Behavior of this sort is consistent with that noted in the experiments of Ref. 1. However, attempts to reproduce this behavior theoretically, with system parameters based on the experiments, were not successful.

Since the type of panel considered here is far from a realistic one, no firm conclusions can be drawn regarding the practical impact of nonlinear hypersonic loading. However, it is clear that any assessment of this effect should include an accurate determination of the true in-plane restraint condition. A flat panel of finite span, which is also stabilized by stretching in the spanwise direction, should be less susceptible to nonlinear hypersonic effects in comparison with its two-dimensional counterpart. The introduction of curvature, particularly as far as shells are concerned, presents a different situation. It has been found (Ref. 16) that a nonlinear structural shell model, with linear aerodynamic loading, exhibits a "softening" nonlinear behavior of the same type as is produced

by nonlinear aerodynamic loading for the flat panels studied in this paper. The introduction of nonlinear aerodynamic loading into a shell analysis could very well reinforce significantly this behavior. Finally, there is the question of viscous aerodynamic effects. Within a linear framework, viscous effects on panel flutter are generally thought to be most important for Mach numbers near unity (Ref. 17). It is simply not known if this situation will change when nonlinear aerodynamic loading is significant.

A new perturbation method for nonlinear oscillations has been applied to a two-mode model of a panel with hypersonic aerodynamic loading. This method is capable of generating recursively approximations to the asymptotic behavior of the panel. The differential equations produced are simple enough to be integrated analytically, although the algebra involved is quite complicated. Fortunately, there is enough organization to the algebra that it can be performed relatively easily by computers. Once this software is set up, parameter surveys can readily be performed, and the variation of the panel stability characteristic with system parameters is displayed with enhanced clarity in comparison with the information obtained from direct integration. Although the analytical results are capable of demonstrating the amplitude-sensitive instability, the one numerical example that was attempted indicated that for the parameters chosen this instability would not occur. A final judgment concerning the utility and accuracy of the perturbation method must await detailed comparisons between the new method's predictions and those obtained from direct integration.

REFERENCES

1. Ketter, D. J. and Voss, H. M., "Panel Flutter Analyses and Experiments in the Mach Number Range of 5.0 to 10.0," FDL-TDR-64-6, March 1964.
2. Bolotin, V. V., Gavrilov, Iu. V., Makarov, B. P., and Shveiko, Iu. Iu., "Nonlinear Problems of the Stability of Plane Panels at Hypersonic Speeds," Izvestiia Akademiia Nauk SSSR, OTN, Mekh. i Mashino., No. 3, 1959, pp. 59-64.
3. Librescu, L., "Aeroelastic Stability of Orthotropic Heterogeneous Thin Panels in the Vicinity of the Flutter Critical Boundary, Part I," Journal de Mecanique, Vol. 4, No. 1, March 1965, pp. 51-76.
4. Eastep, F. E. and McIntosh, S. C., Jr., "Analysis of Nonlinear Panel Flutter and Response under Random Excitation or Nonlinear Aerodynamic Loading," AIAA Journal, Vol. 9, No. 3, March 1971, pp. 411-418.
5. McIntosh, S. C., Jr., "The Effect of Hypersonic Nonlinear Aerodynamic Loading on Panel Flutter," AIAA Journal, Vol. 11, No. 1, January 1973, pp. 29-32.
6. Lerner, J. I., "Unsteady Viscous Effects in the Flow over an Oscillating Surface," SUDAAR No. 453, December 1972, Dept. of Aeronautics and Astronautics, Stanford University, Stanford, CA.
7. McIntosh, S. C., Jr., "Preliminary Theoretical Considerations of Some Nonlinear Aspects of Hypersonic Panel Flutter," Annual Report, 1 September 1965 to 31 August 1966, NASA Grant NGR 05-020-102, Dept. of Aeronautics and Astronautics, Stanford University, Stanford, CA.
8. McIntosh, S. C., Jr., "Theoretical Considerations of Some Nonlinear Aspects of Hypersonic Panel Flutter," Second Annual Report, 1 September 1966 to 31 August 1967, NASA Grant NGR 05-020-102, Dept. of Aeronautics and Astronautics, Stanford University, Stanford, CA.
9. McIntosh, S. C., Jr. and Lerner, J. I., "Theoretical Considerations of Some Nonlinear Aspects of Hypersonic Panel Flutter," Third Annual Report, 1 September 1967 to 31 August 1968, NASA Grant NGR 05-020-102,

Dept. of Aeronautics and Astronautics, Stanford University, Stanford, CA.

10. McIntosh, S. C., Jr. and Lerner, J. I., "Theoretical Considerations of Some Nonlinear Aspects of Hypersonic Panel Flutter," Fourth Annual Report, 1 September 1968 to 31 August 1969, NASA Grant NGR 05-020-102, Dept. of Aeronautics and Astronautics, Stanford University, Stanford, CA.
11. Dowell, E. H., "Nonlinear Oscillations of a Fluttering Plate," AIAA Journal, Vol. 4, No. 7, July 1966, pp. 1267-1275.
12. La Salle, J. and Lefschetz, S., Stability by Liapunov's Direct Method With Applications, Academic Press, New York, 1961, pp. 30-33.
13. Dimantha, P. C. and Roorda, J., "On the Domain of Asymptotic Stability of Nonlinear Nonconservative Systems," Applied Scientific Research, Vol. 20, March 1969, pp. 272-288.
14. Kamel, A. A., "Perturbation Method in the Theory of Nonlinear Oscillations," Celestial Mechanics, Vol. 3, No. 1, 1970, pp. 90-106.
15. Morino, L., "A Perturbation Method for Treating Nonlinear Panel Flutter Problems," AIAA Journal, Vol. 7, No. 3, March 1969, pp. 405-411.
16. Evensen, D. A. and Olson, M. D., "Nonlinear Flutter of a Circular Cylindrical Shell in Supersonic Flow," NASA TN D-4265, December 1967.
17. Dowell, E. H., "Panel Flutter: A Review of the Aeroelastic Stability of Plates and Shells," AIAA Journal, Vol. 8, No. 3, March 1970, pp. 385-399.

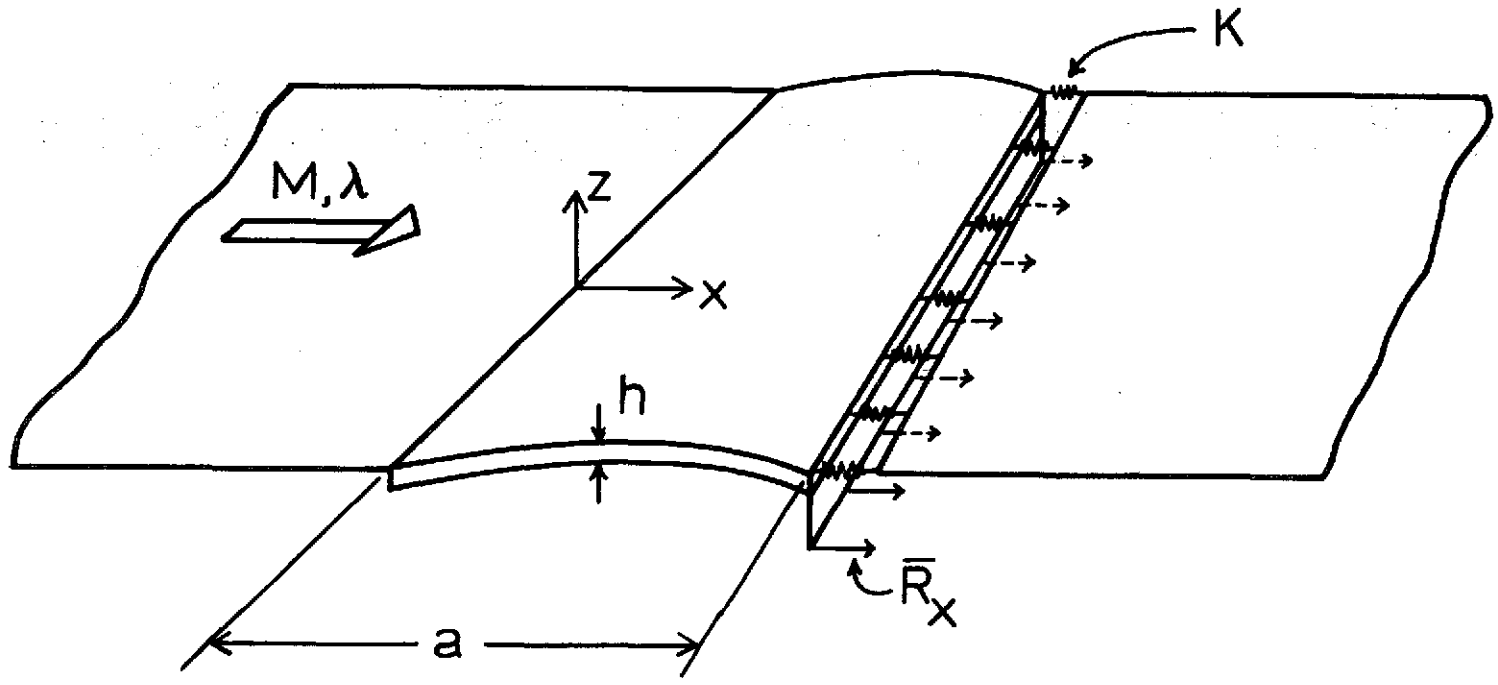

Figure 1. Two-dimensional panel (plate-column) on hinged supports.

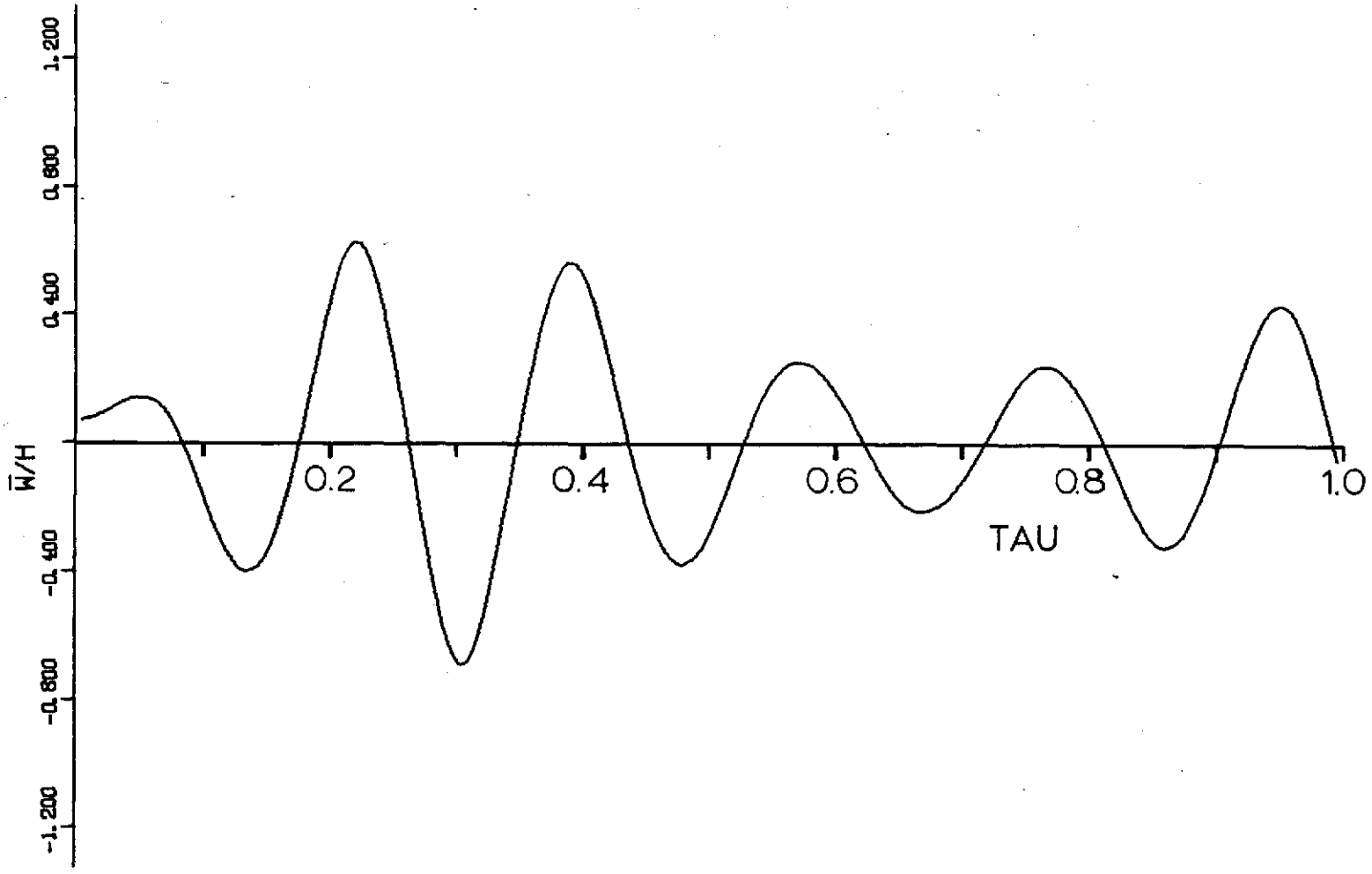

Figure 2. Dimensionless panel displacement at $x = 0.75a$ vs. dimensionless time τ; $\lambda = 400$, $\frac{\mu}{M} = 0.01$, $\alpha = 1.0$, $N = 6$, $a_1(0) = 0.1$, linear aerodynamic terms.

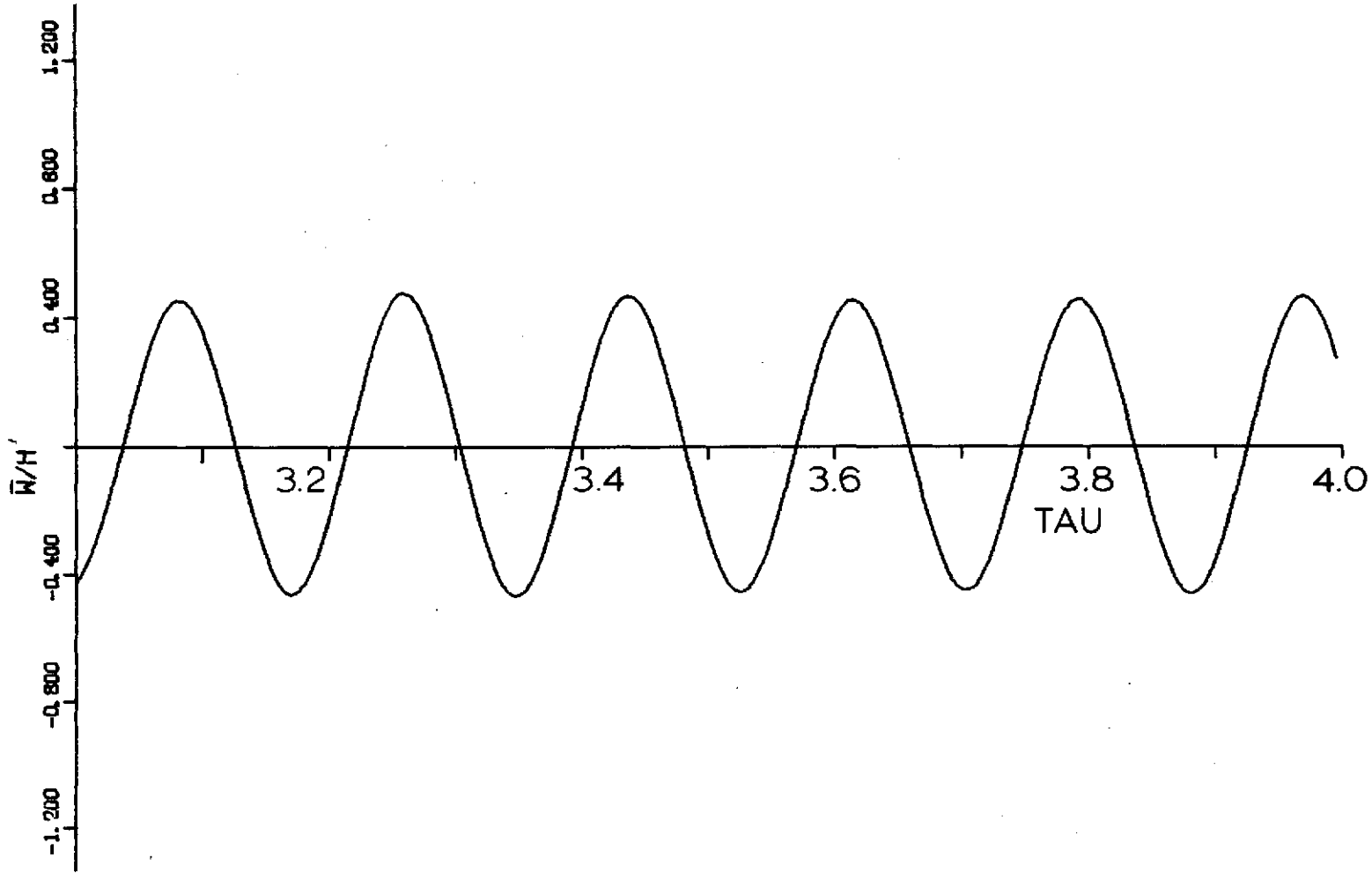

Figure 3. Continuation, response of panel of Fig. 2.

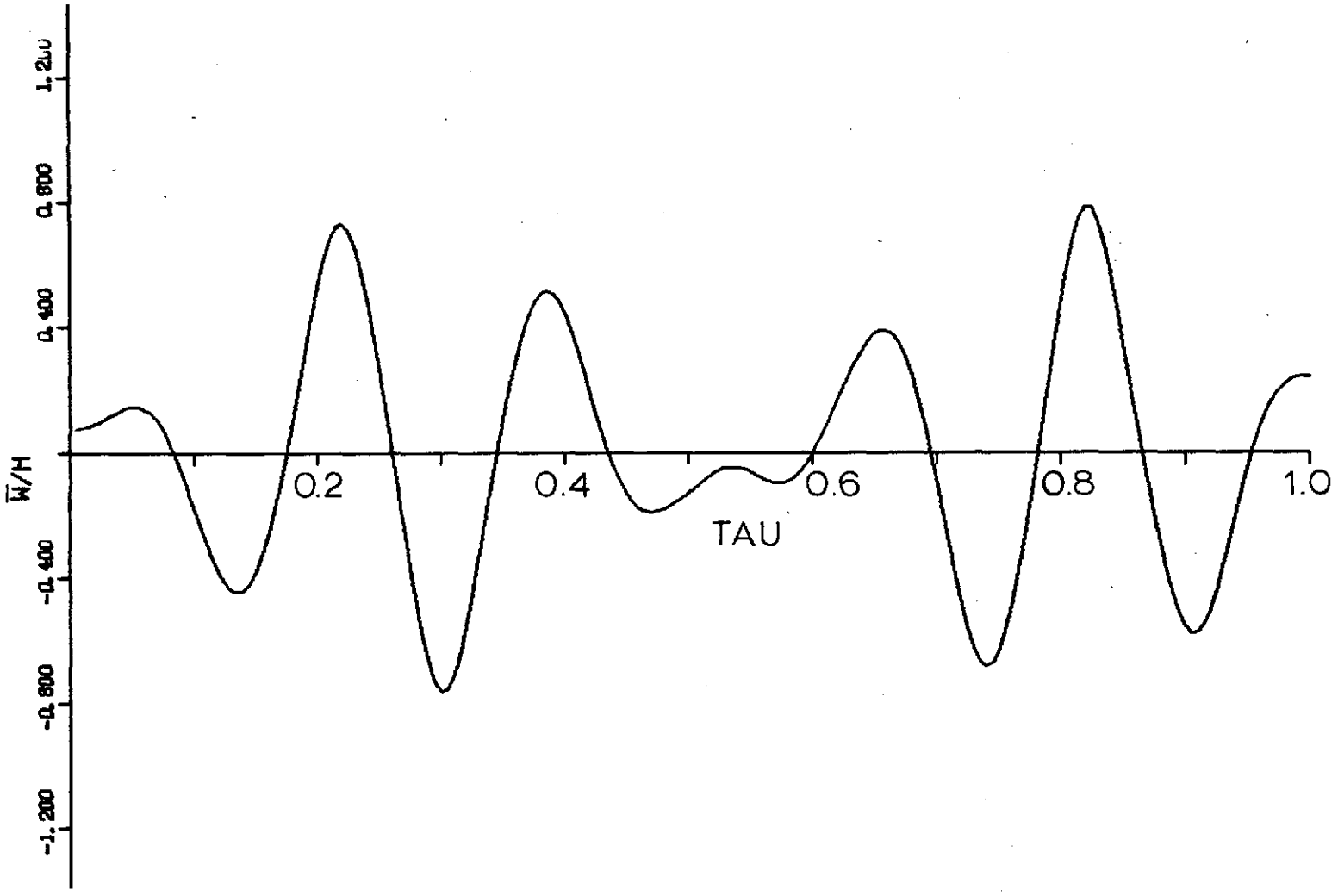

Figure 4. Dimensionless panel displacement at $x = 0.75a$ vs. dimensionless time τ for zero system damping; $\lambda = 400$, $\frac{\mu}{M} = 0.0$, $\alpha = 1.0$, $N = 6$, $a_1(0) = 0.1$, linear aerodynamic terms.

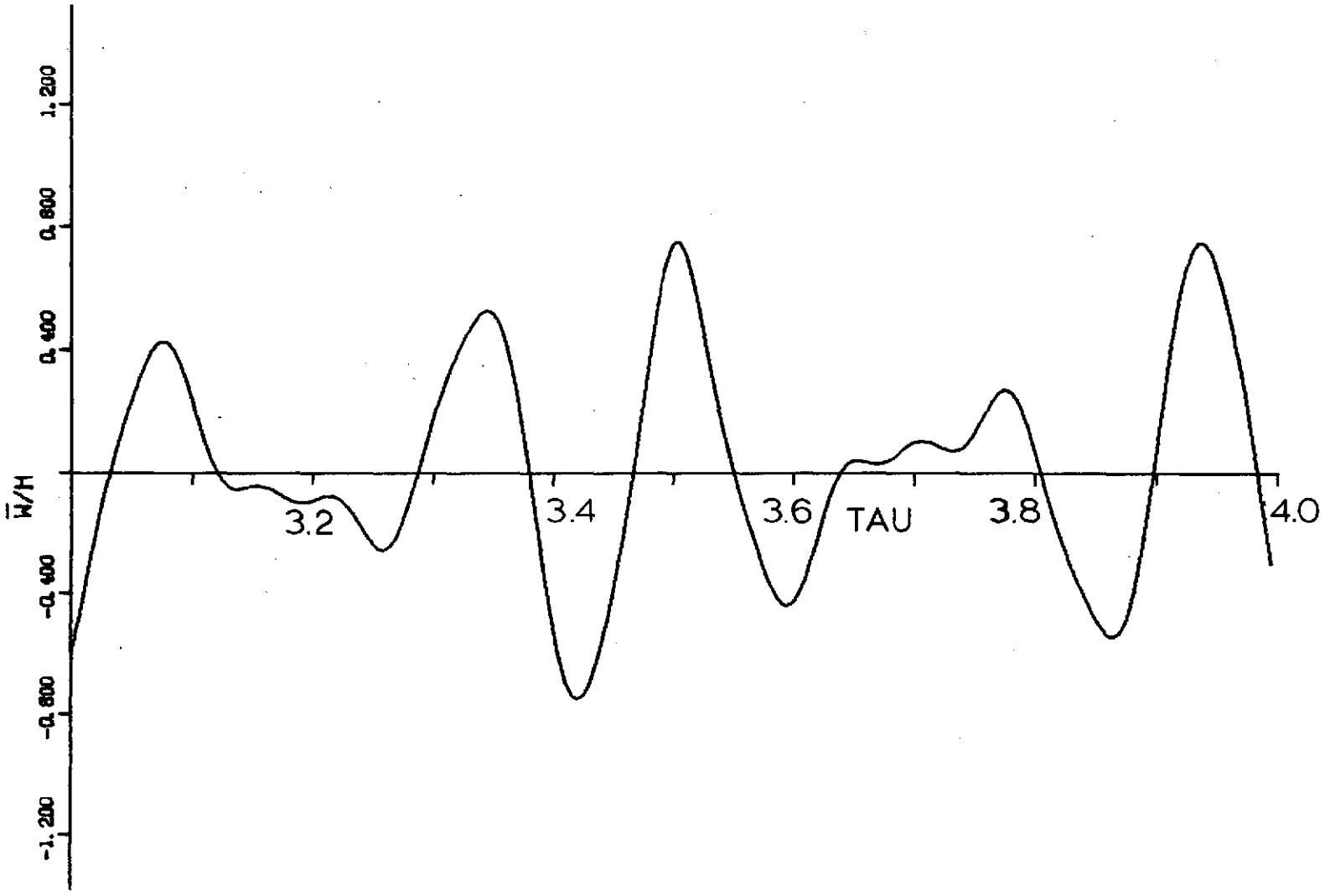

Figure 5. Continuation, response of panel of Fig. 4.

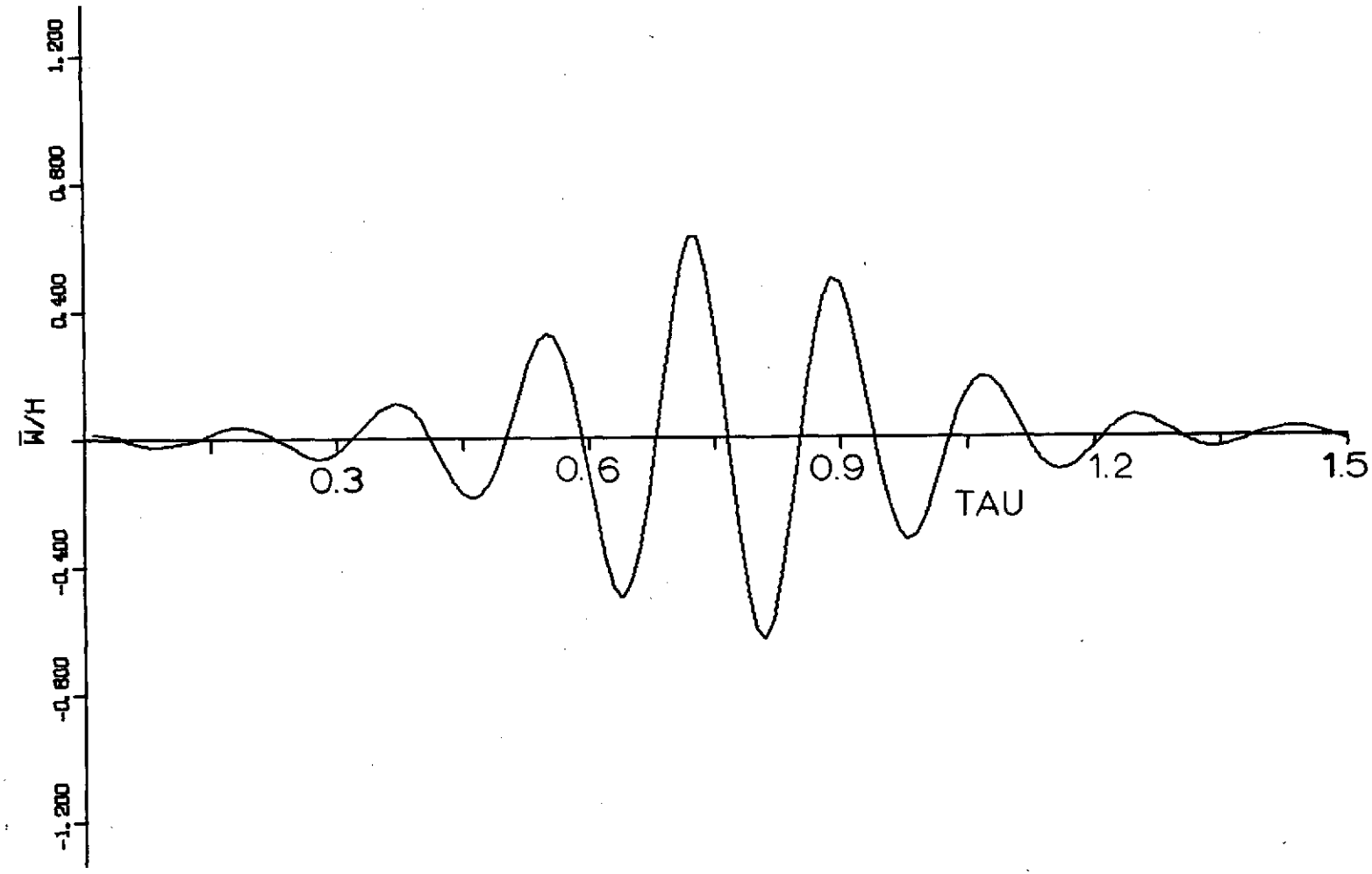

Figure 6. Dimensionless panel displacement at $x = 0.75a$ vs. dimensionless time τ for zero system damping; $\lambda = 400$, $\frac{\mu}{M} = 0.0$, $\alpha = 1.0$, $N = 6$, $a_1(0) = -a_2(0) = 0.01$, linear aerodynamic terms.

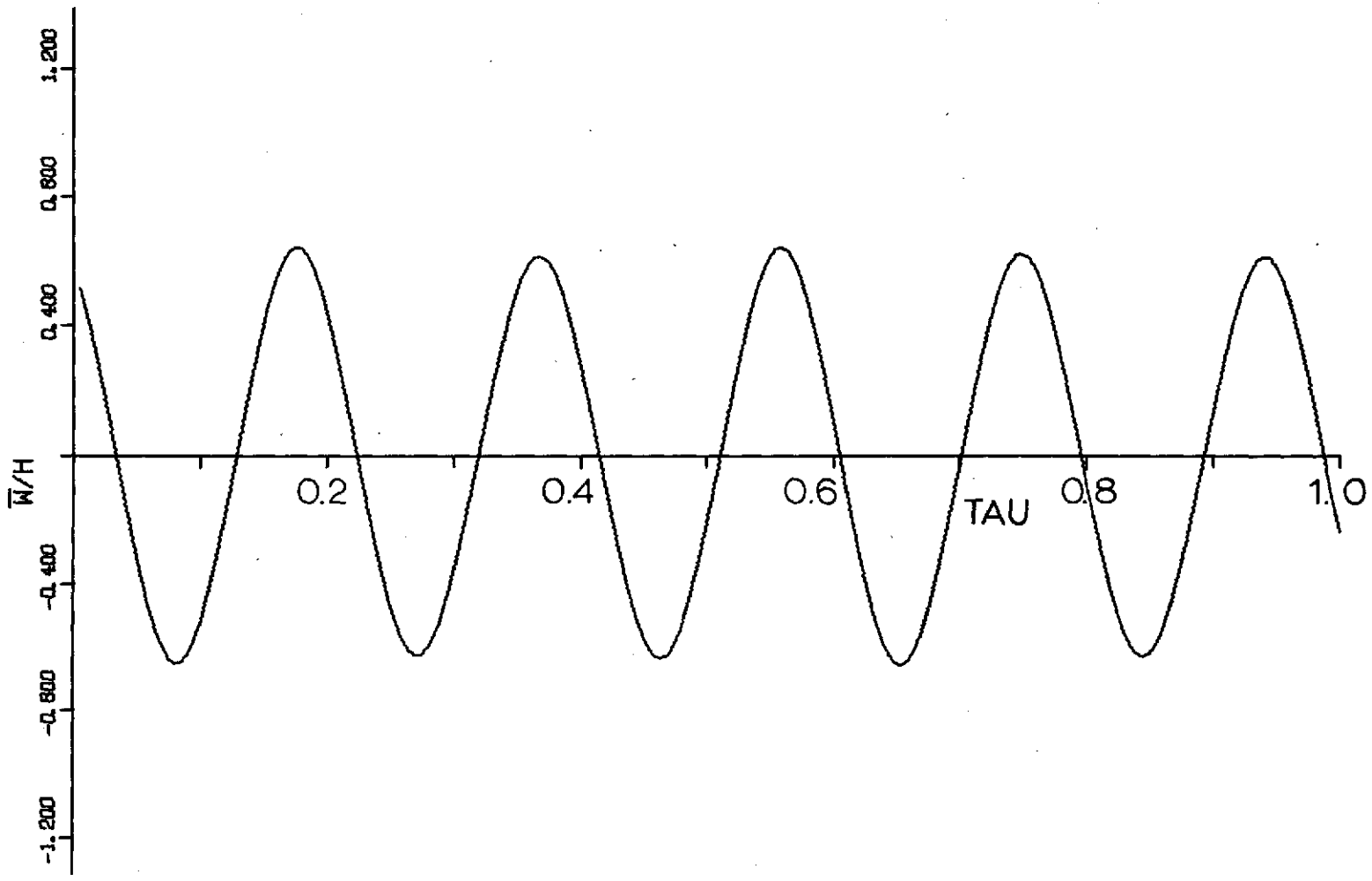

Figure 7. Dimensionless panel displacement at $x = 0.75a$ vs. dimensionless time τ for zero system damping; $\lambda = 346.1$, $\frac{\mu}{M} = 0.0$, $\alpha = 1.0$, $N = 2$, $a_1(0) = -a_2(0) = 0.363$, linear aerodynamic terms.

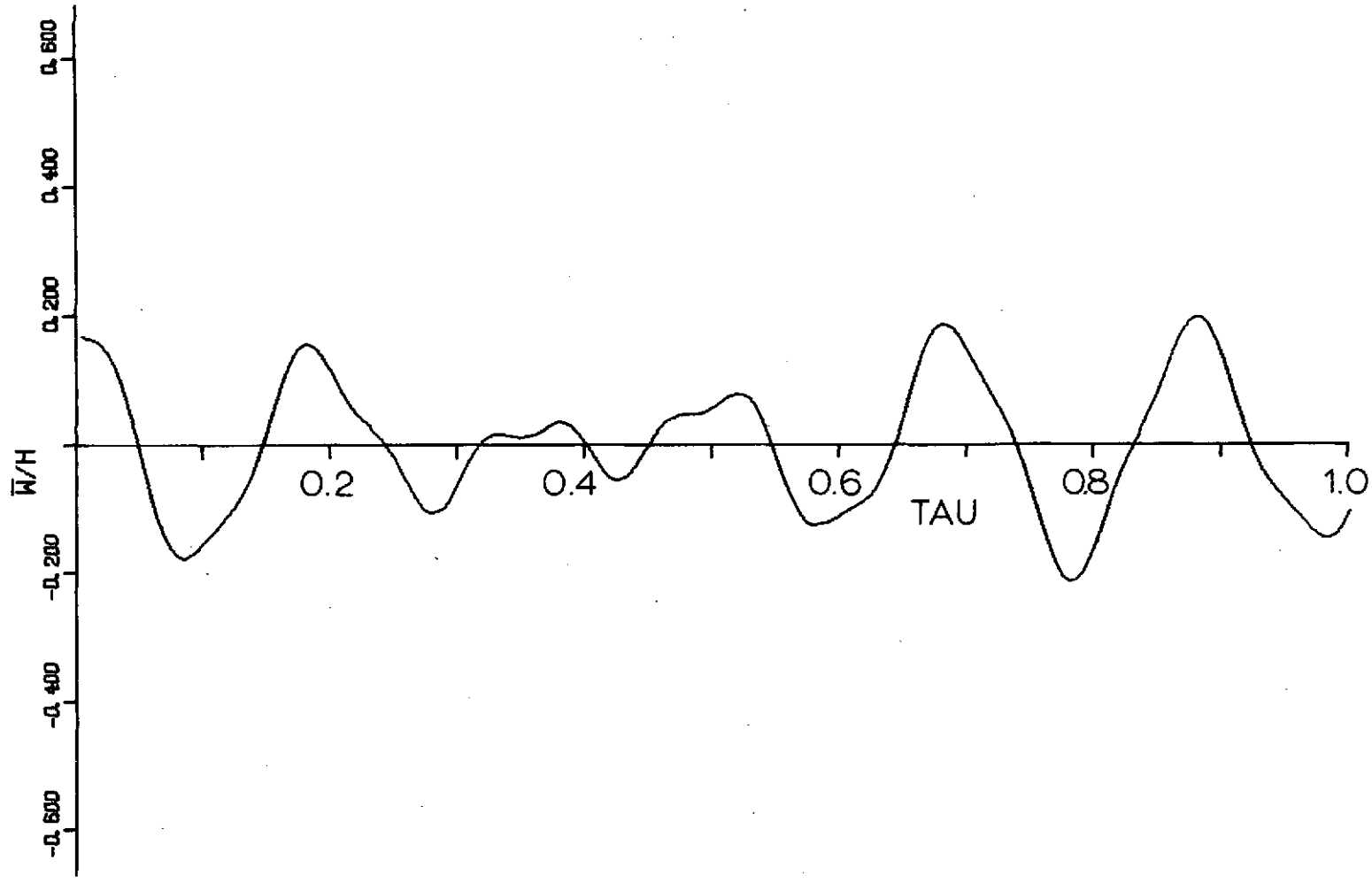

Figure 8. Dimensionless panel displacement at $x = 0.75a$ vs. dimensionless time τ for zero system damping and subcritical λ; $\lambda = 330$, $\frac{\mu}{M} = 0.0$, $\alpha = 1.0$, $N = 6$, $a_1(0) = -a_2(0) = 0.1$, linear aerodynamic terms.

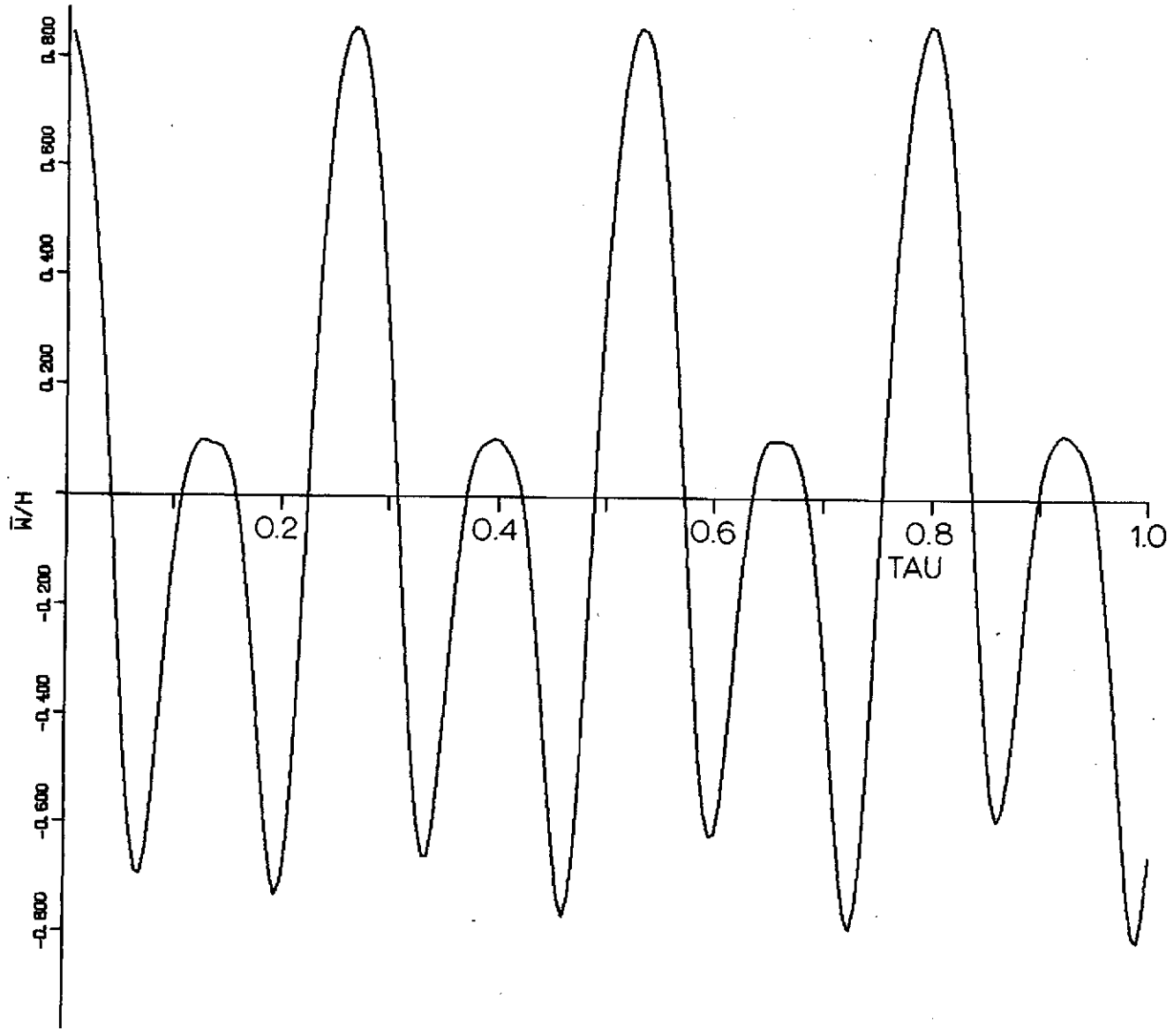

Figure 9. Response of panel of Fig. 8 with different initial conditions — $a_1(0) = -a_2(0) = 0.5$.

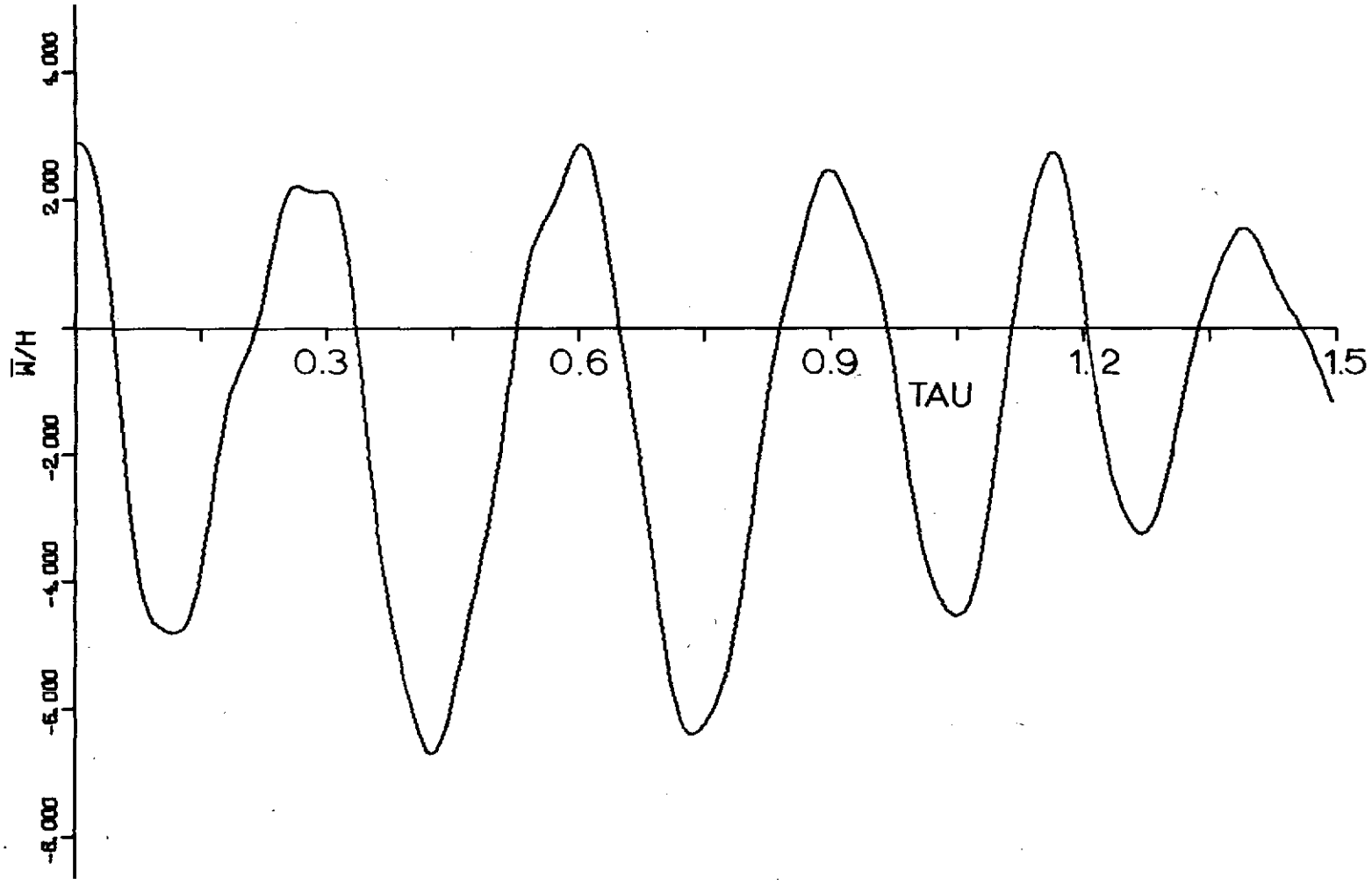

Figure 10. Dimensionless panel displacement at $x = 0.75a$ vs. dimensionless time τ; $\lambda = 330$, $\frac{\mu}{M} = 0.01$, $\alpha = 0.0$, $N = 6$, $\frac{Mh}{a} = 0.05$, $a_1(0) = -a_2(0) = 1.71$, linear aerodynamic terms plus term proportional to $\left(\frac{\partial \bar{w}}{\partial x}\right)^2$ from $(F_z)_k$.

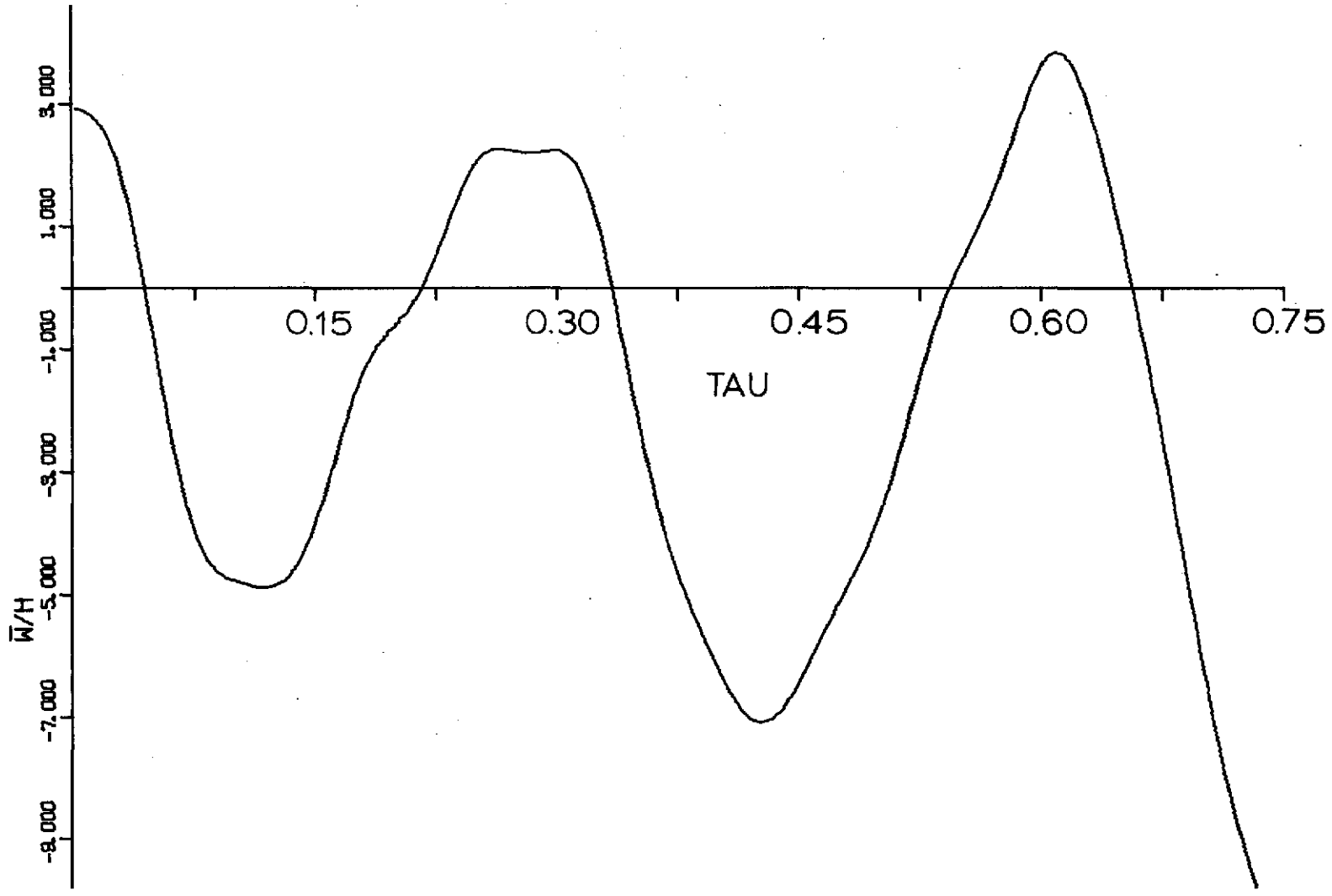

Figure 11. Response of panel of Fig. 10 with slightly greater initial conditions — $a_1(0) = -a_2(0) = 1.72$.

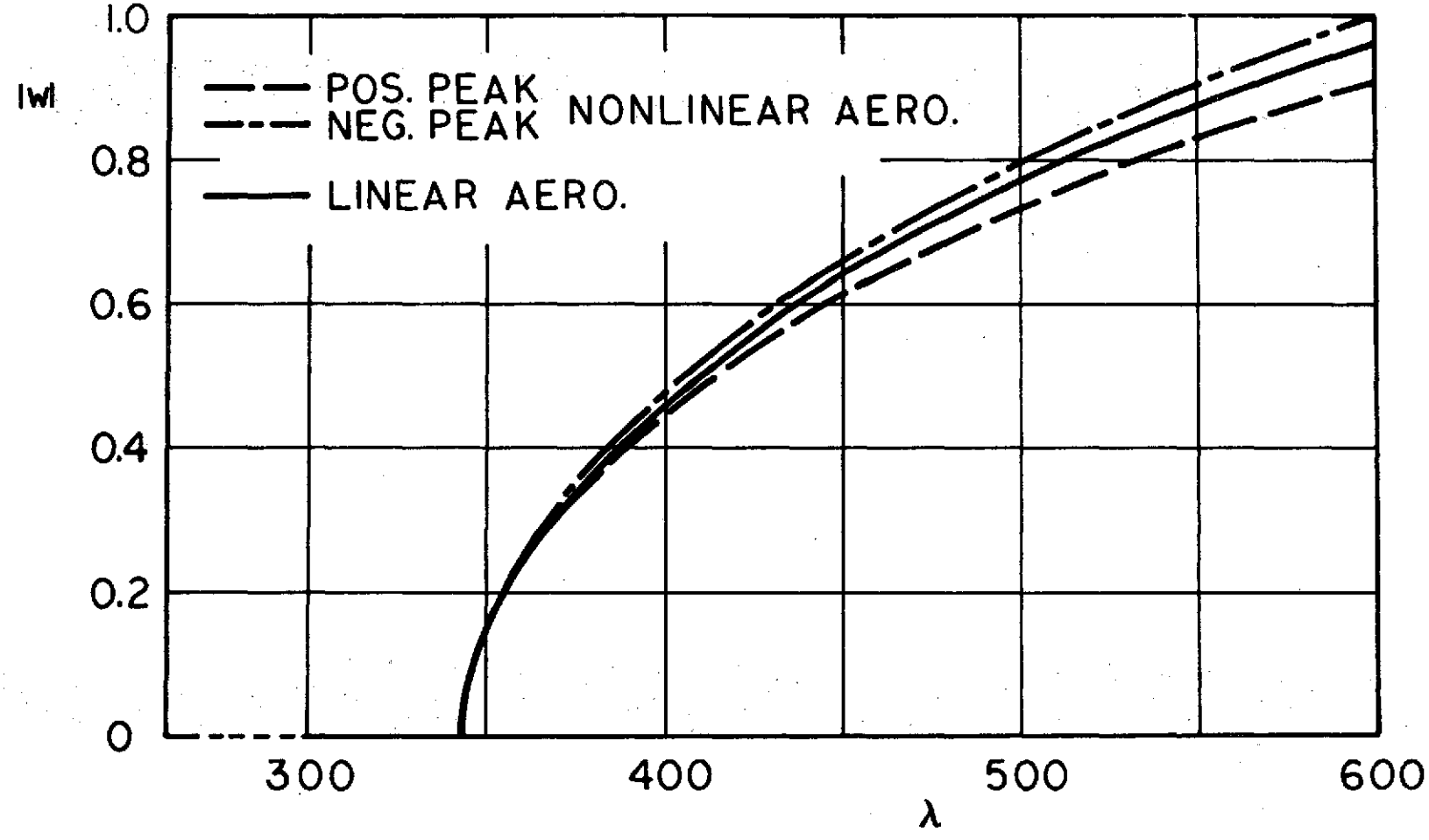

Figure 12. Maximum absolute value of dimensionless panel displacement w at $x/a = 0.75$ versus dimensionless dynamic pressure λ; $N = 6$, $R_x = 0$, $\alpha = 1$, $\mu/M = 0.01$, $\Delta p = 0$, $Mh/a = 0.05$. Nonlinear aerodynamic loading made up of piston-theory terms proportional to $(\partial\overline{w}/\partial x)^2$ and $(\partial\overline{w}/\partial x)(\partial\overline{w}/\partial t)$.

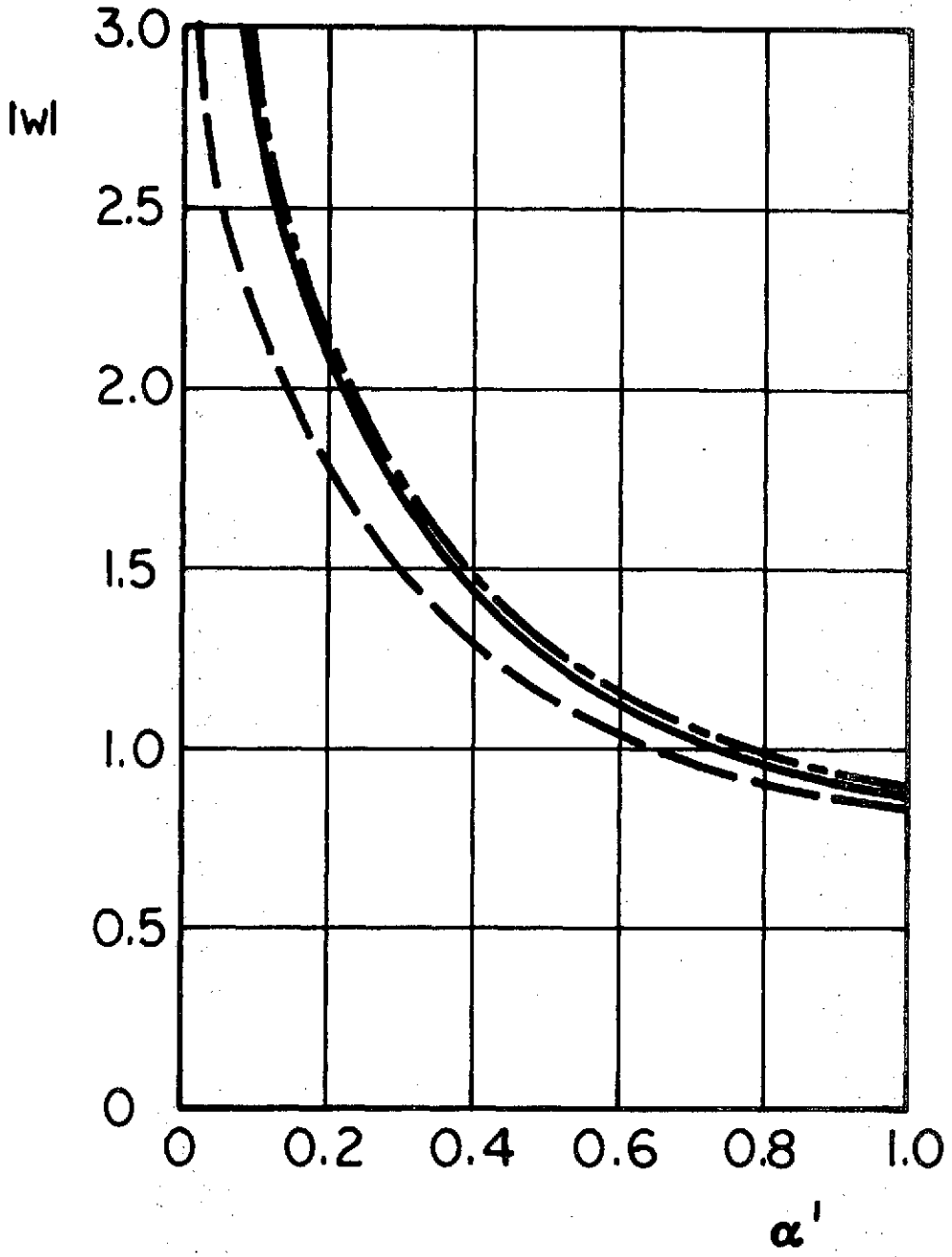

Figure 13. Maximum absolute value of dimensionless panel displacement w at $x/a = 0.75$ versus in-plane restraint parameter α, for $\lambda = 550$. Other parameters and curve legend same as in Fig. 12.

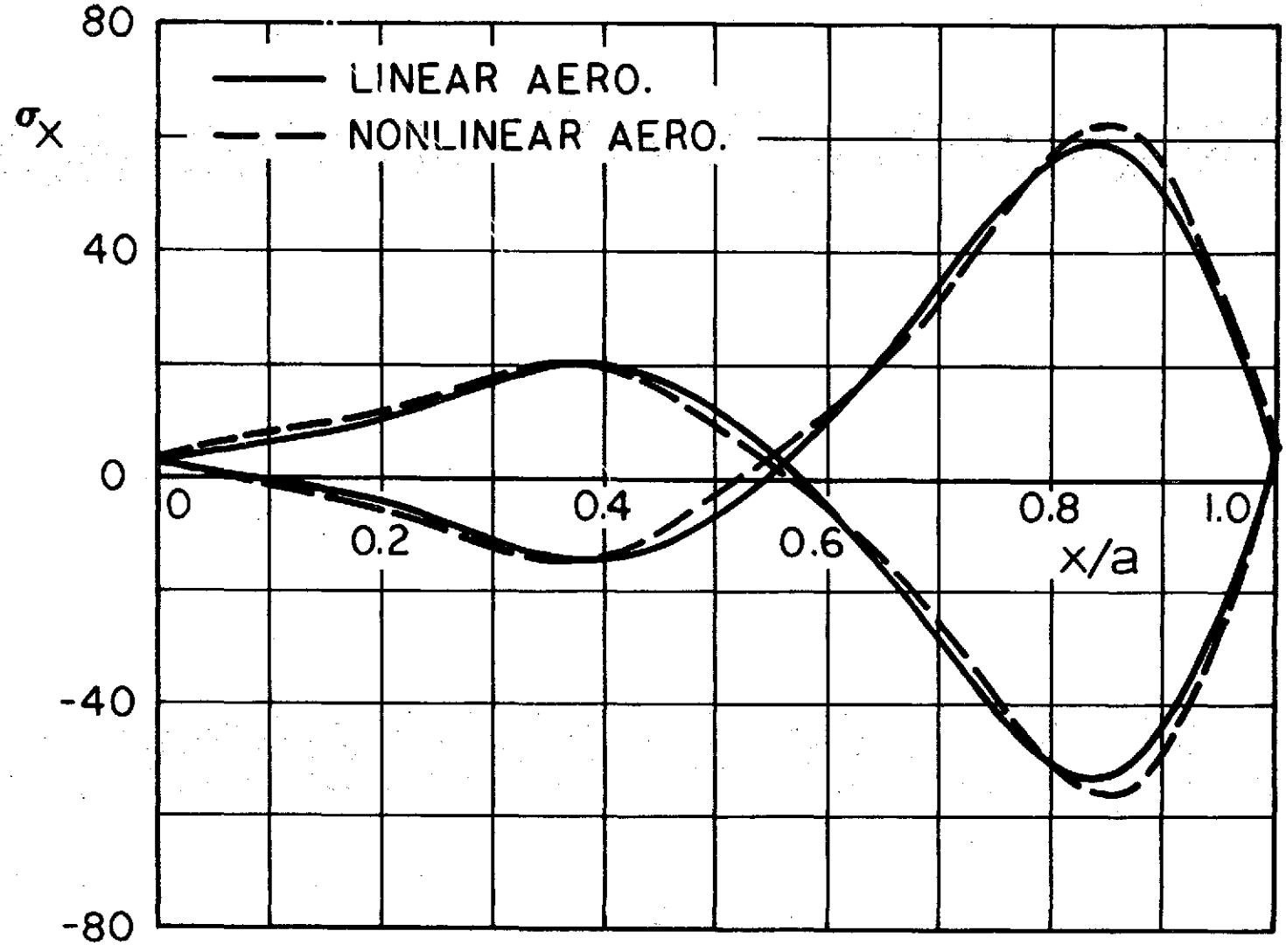

Figure 14. Dimensionless stress σ_x at $z = \pm h/2$ versus chord distance x/a, for $\alpha = 0.1$, $\lambda = 550$, and other parameters as listed for Fig. 12. Stress distributions correspond to peak displacements plotted in Fig. 13, with that due to nonlinear aerodynamic loading calculated for negative (into-cavity) peak.

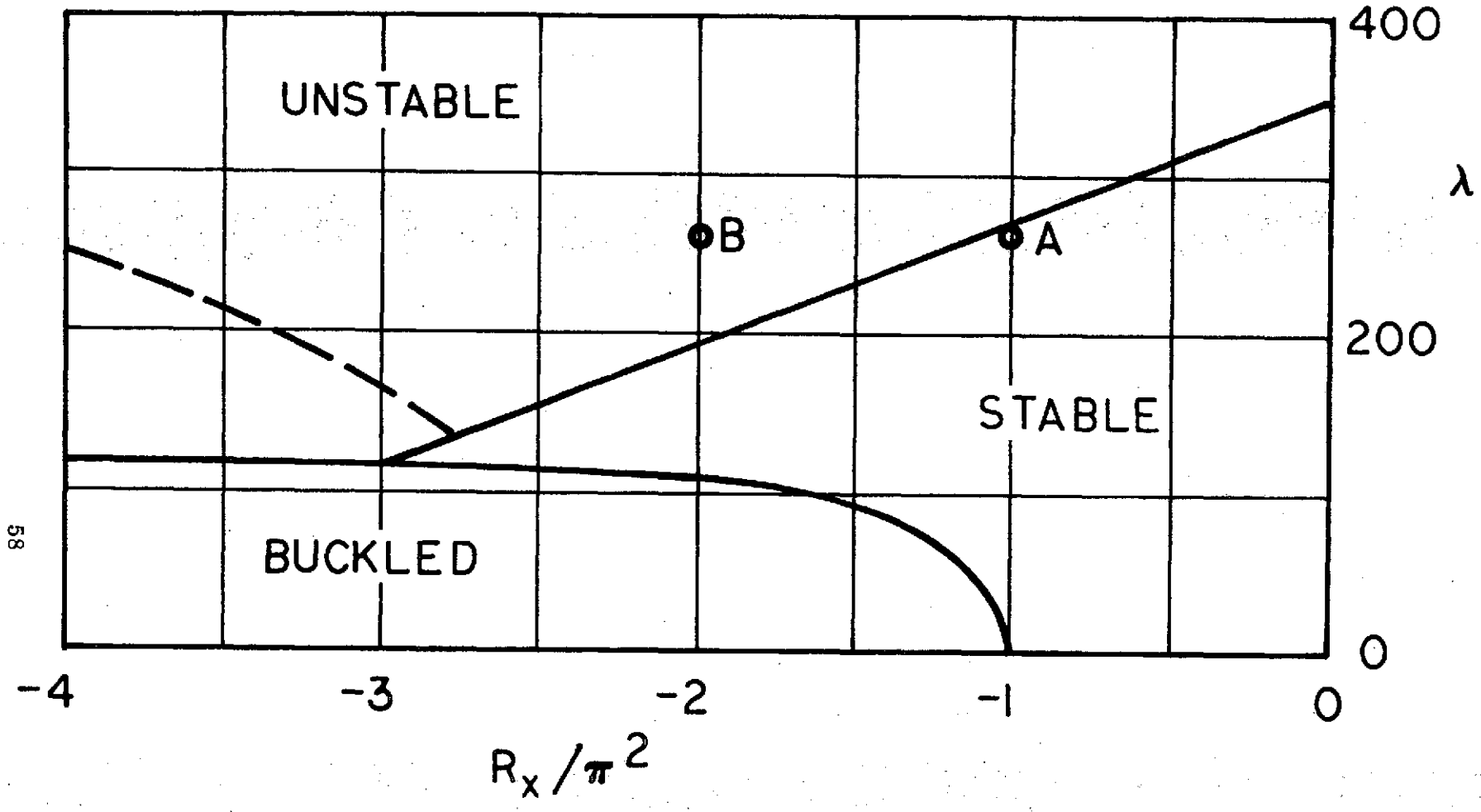

Figure 15. Linear stability boundary for a panel (plate-column) on hinged supports. Ordinate is dimensionless dynamic pressure, abscissa is dimensionless in-plane applied load (negative when panel is in compression). (After Ref. 11.)

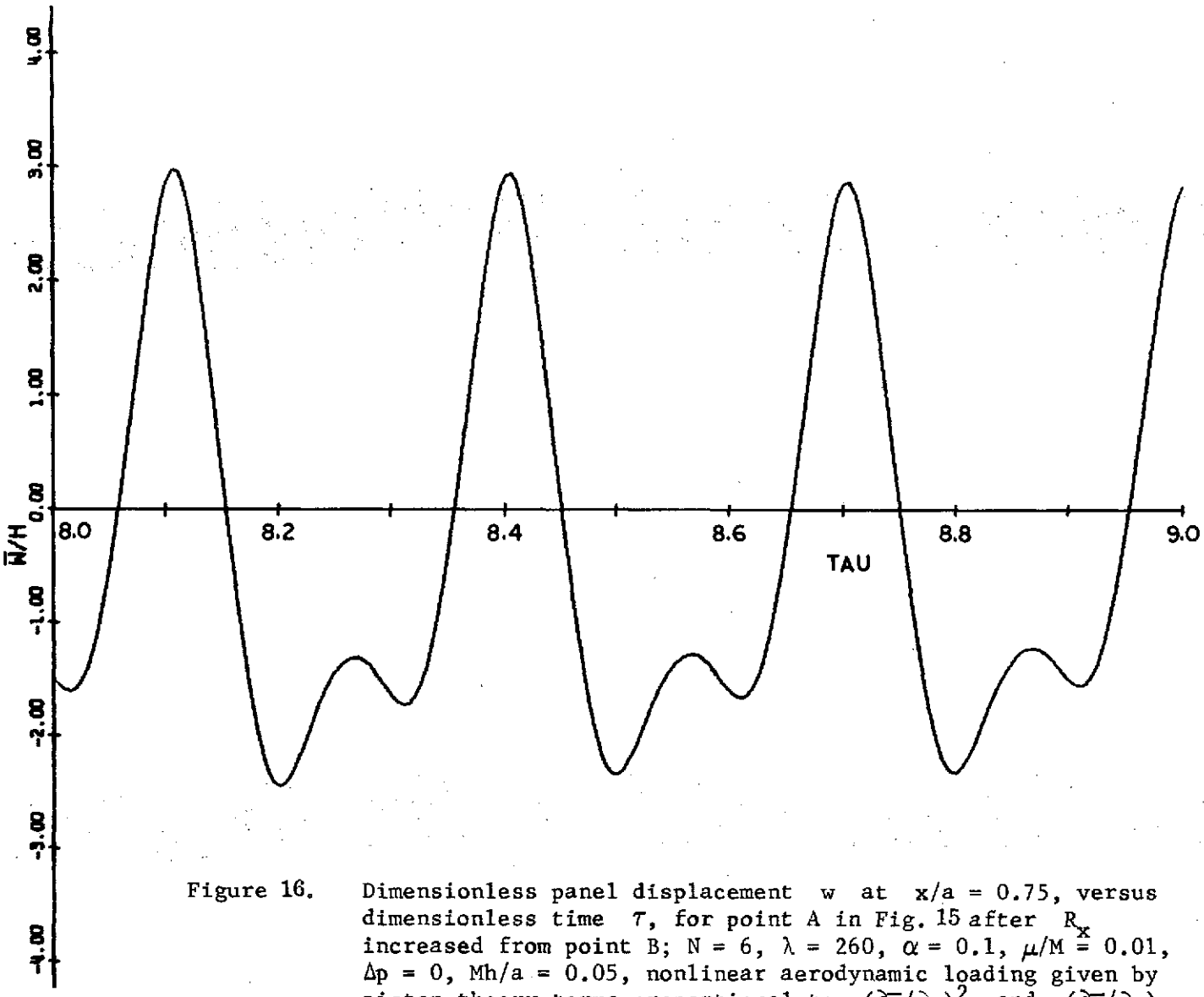

Figure 16. Dimensionless panel displacement w at $x/a = 0.75$, versus dimensionless time τ, for point A in Fig. 15 after R_x increased from point B; $N = 6$, $\lambda = 260$, $\alpha = 0.1$, $\mu/M = 0.01$, $\Delta p = 0$, $Mh/a = 0.05$, nonlinear aerodynamic loading given by piston-theory terms proportional to $(\partial\overline{w}/\partial x)^2$ and $(\partial\overline{w}/\partial x)(\partial\overline{w}/\partial t)$.

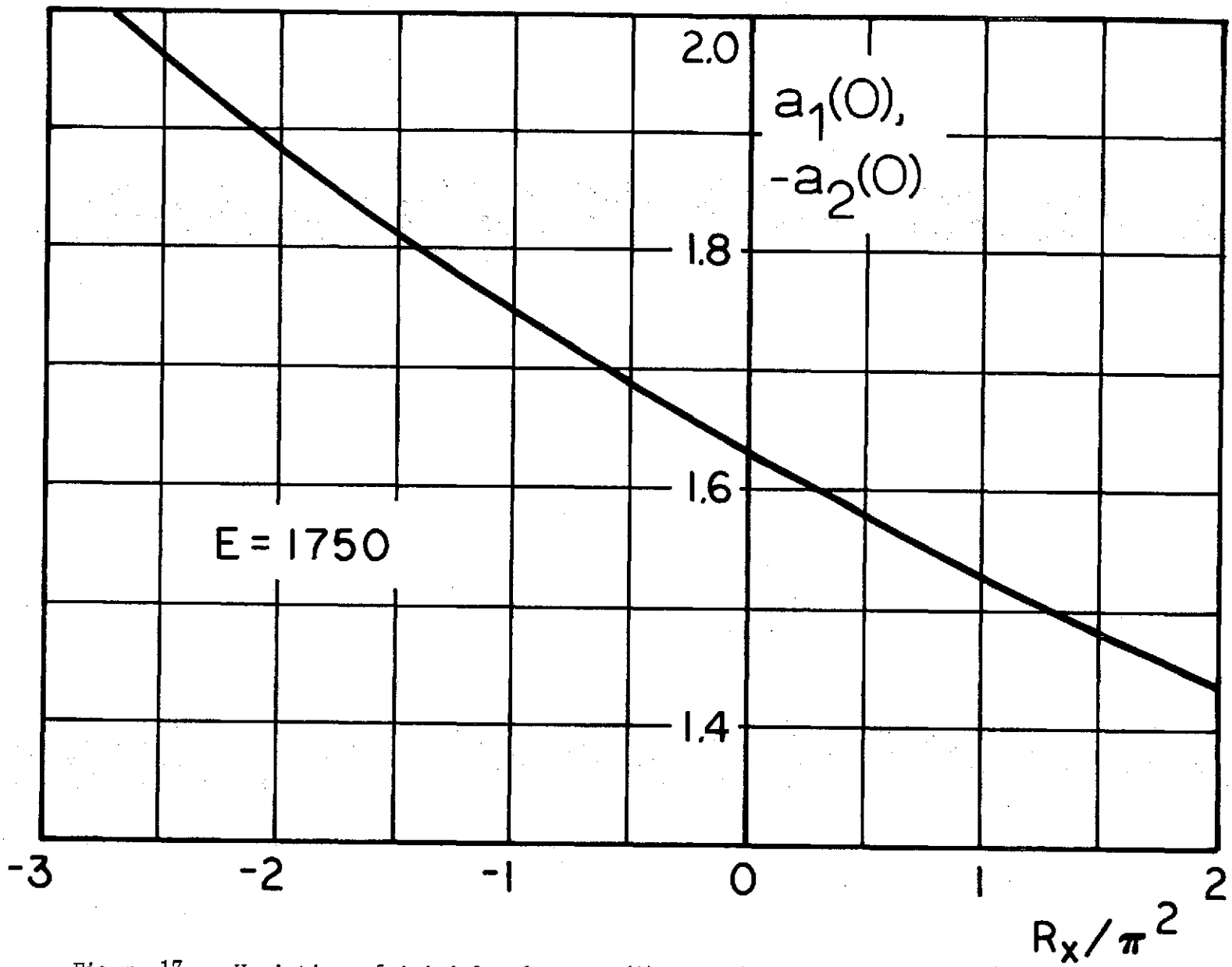

Figure 17. Variation of initial values $a_1(0) = -a_2(0)$ with dimensionless in-plane applied load R_x for $\alpha = 0.1^2$, $E_0 = 1750$.

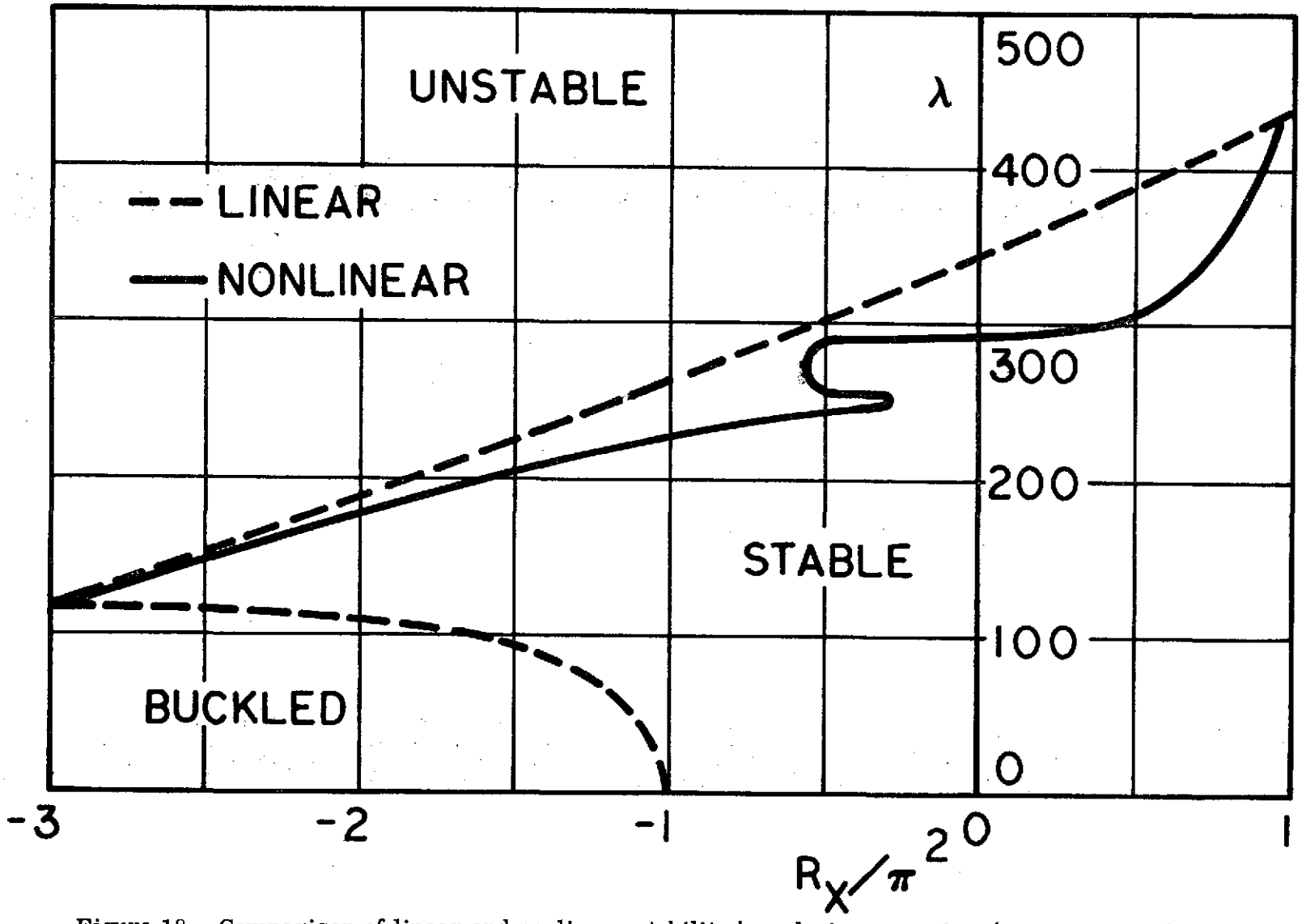

Figure 18. Comparison of linear and nonlinear stability boundaries. $N = 6$, $\mu/M = 0.01$, $Mh/a = 0.05$, $\alpha = 0.1$, $\Delta p = 0$, $E_o = 1750$ with $a_1(0) = -a_2(0) \neq 0$, nonlinear aerodynamic terms proportional to $(\partial\overline{w}/\partial x)^2$ and $(\partial\overline{w}/\partial x)(\partial\overline{w}/\partial t)$.

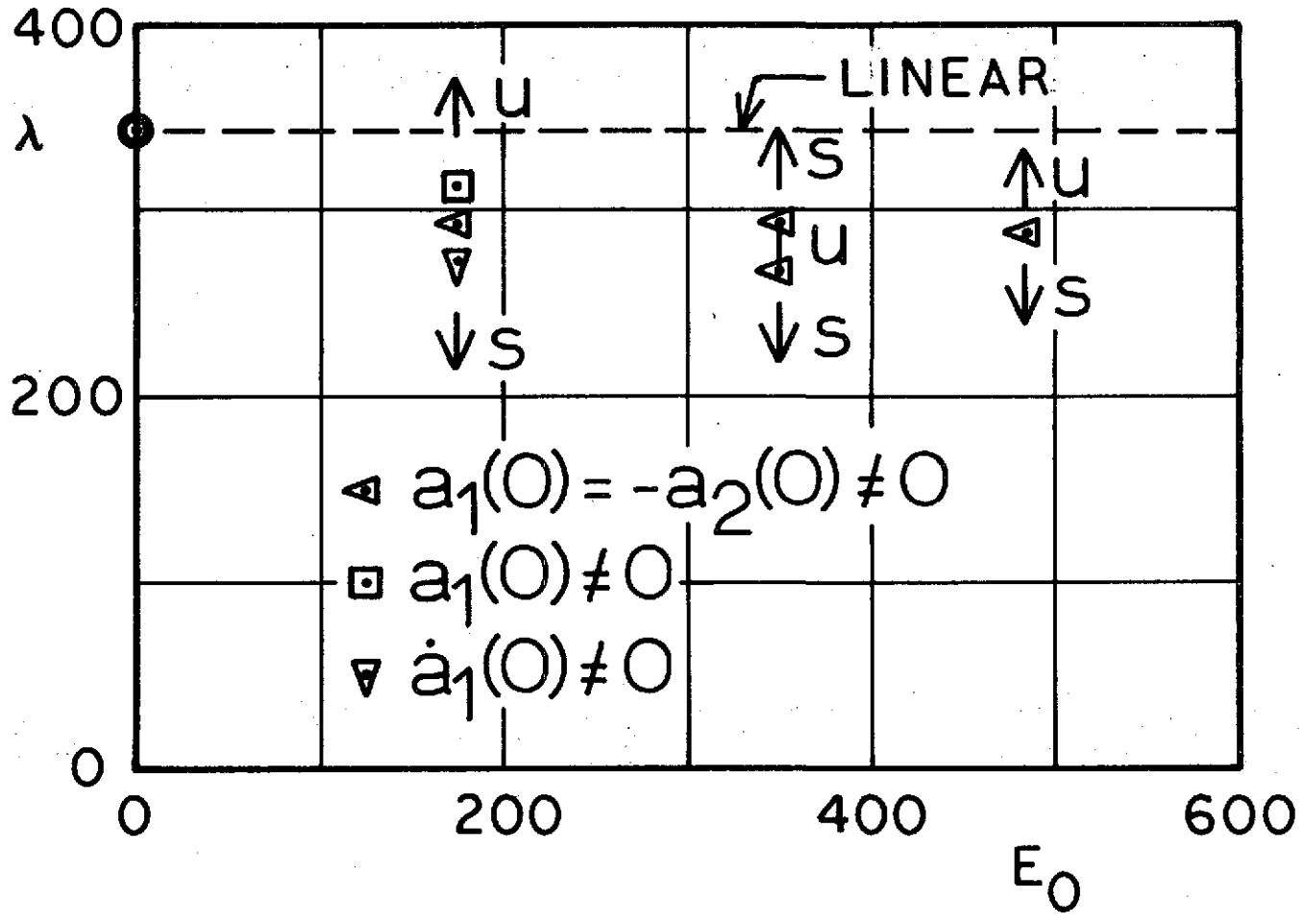

Figure 19. Variation of critical value of λ with initial energy and modal content for $R_x = 0$; other parameters same as in Fig. 18.

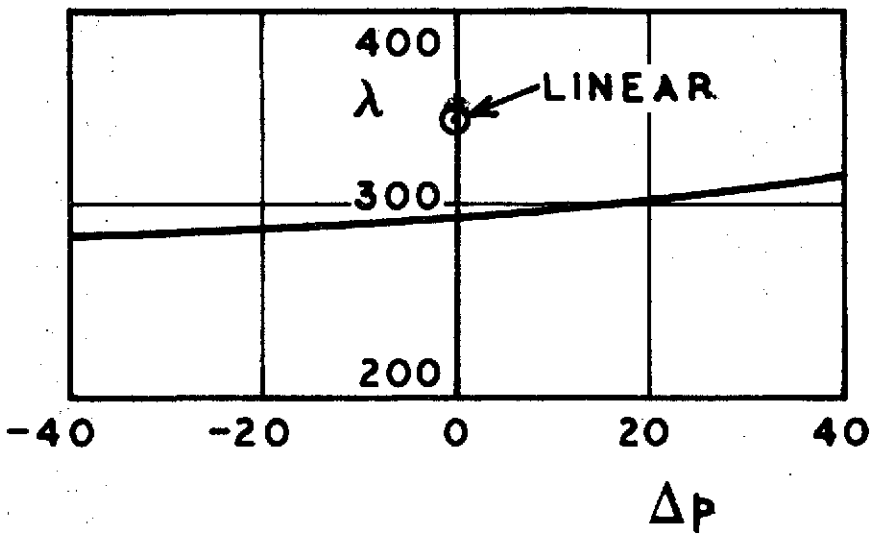

Figure 20. Variation of critical value of λ with dimensionless static pressure difference for fixed initial conditions. $R_x = 0$; other parameters same as in Fig. 18.

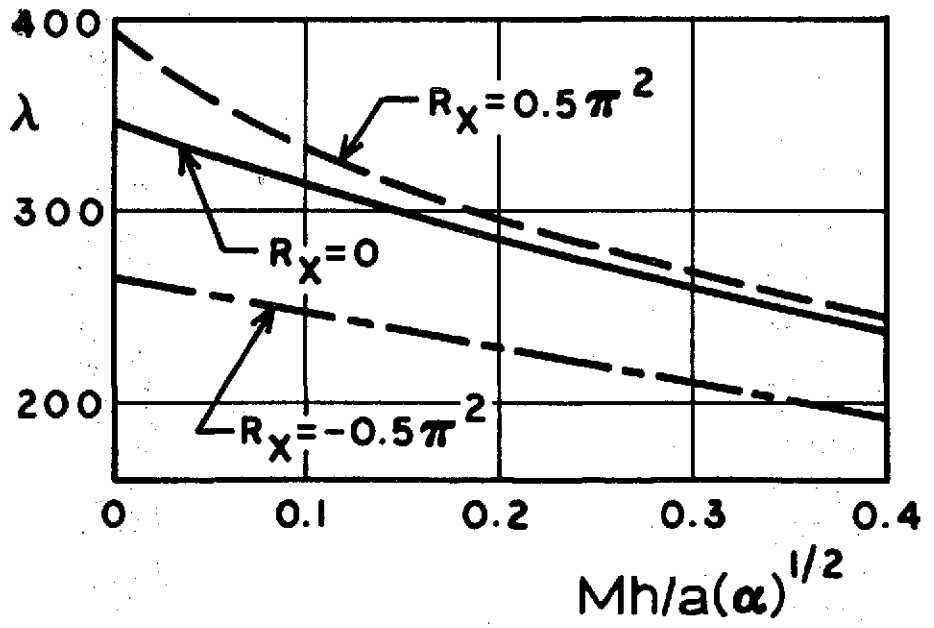

Figure 21. Variation of critical value of λ with nonlinear interaction parameter for $E_o = 1750$, other parameters same as in Fig. 18.